nano-OPID

Yael Maguire, PhD
Visiting Scientist, Harvard

May 1, 2013

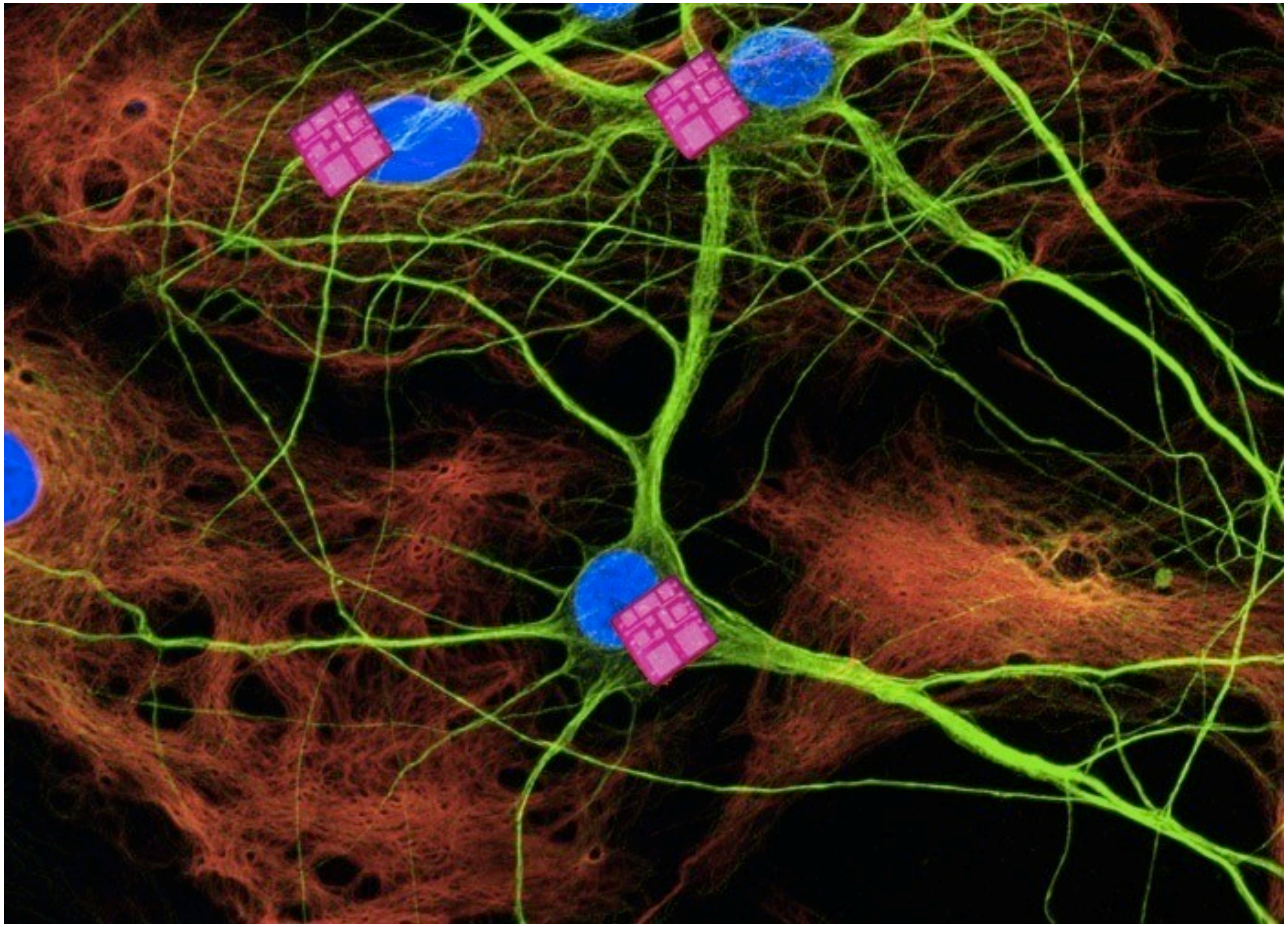

Original confocal image of primary rat hippocampal neurons © Paul Cuddon

At 15 nm feature size, can create more complexity than Intel's original 4004 microprocessor within 100 μm²

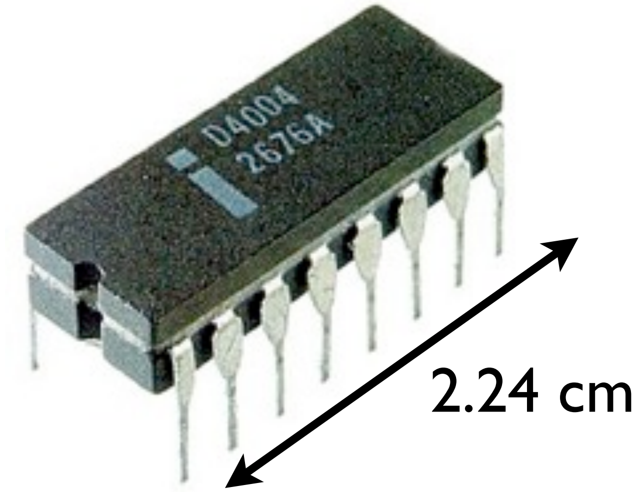

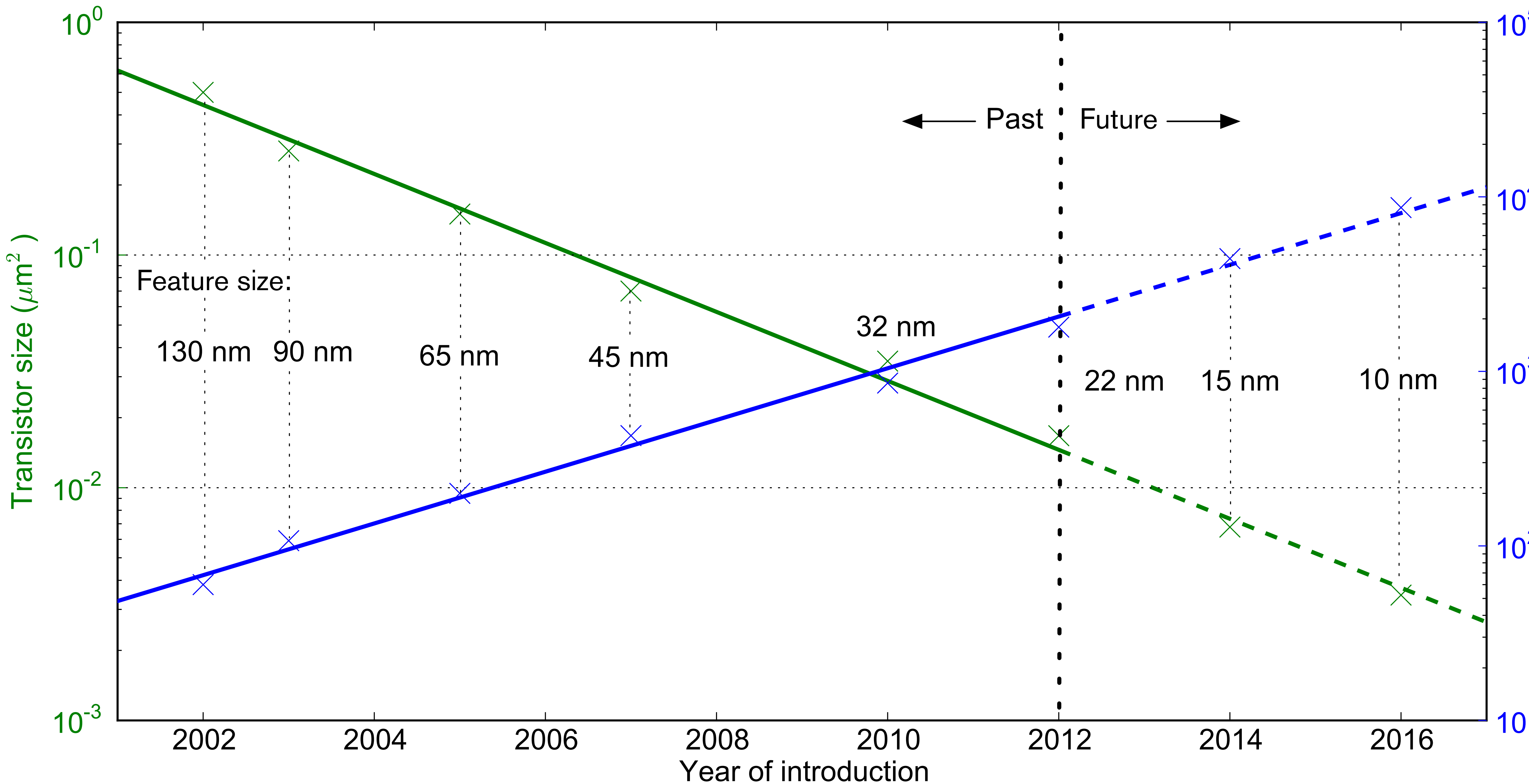

* estimate within 100 μm²

UHF RFID Tag Specifications

- 8-40k gates
- CMOS 0.135 µm (0.414mm x 0.432mm)
- ~10 µW

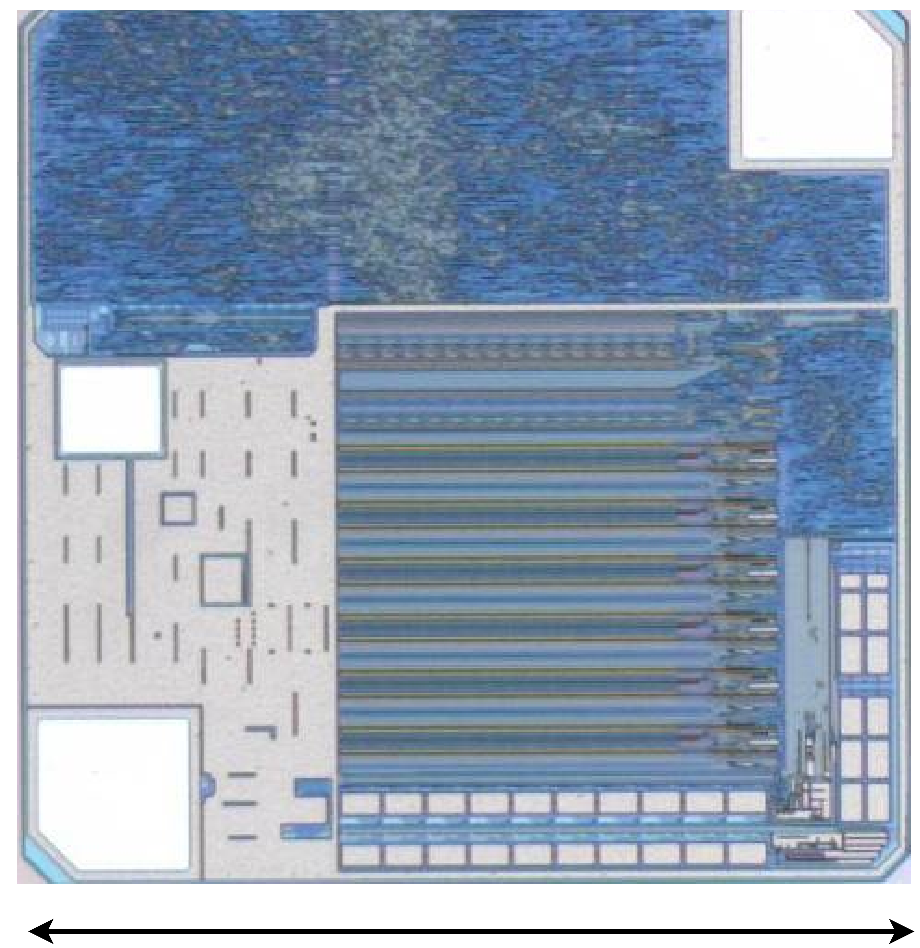

Smaller Systems (2.45 GHz)

Usami, Powder RFID Chip Technology, Nano Letters, v. 7, No. 11, 2007

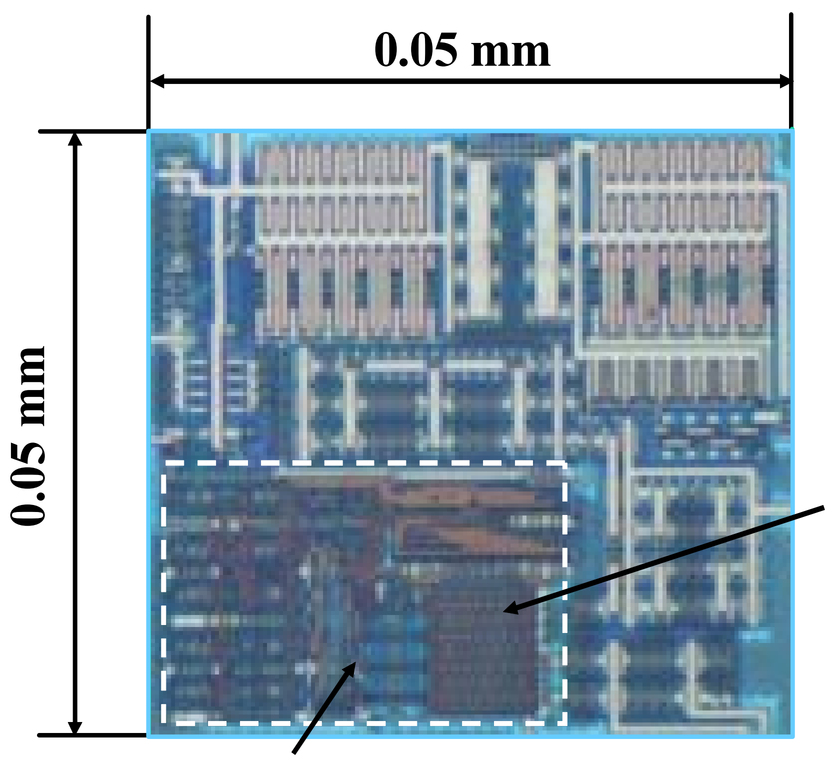

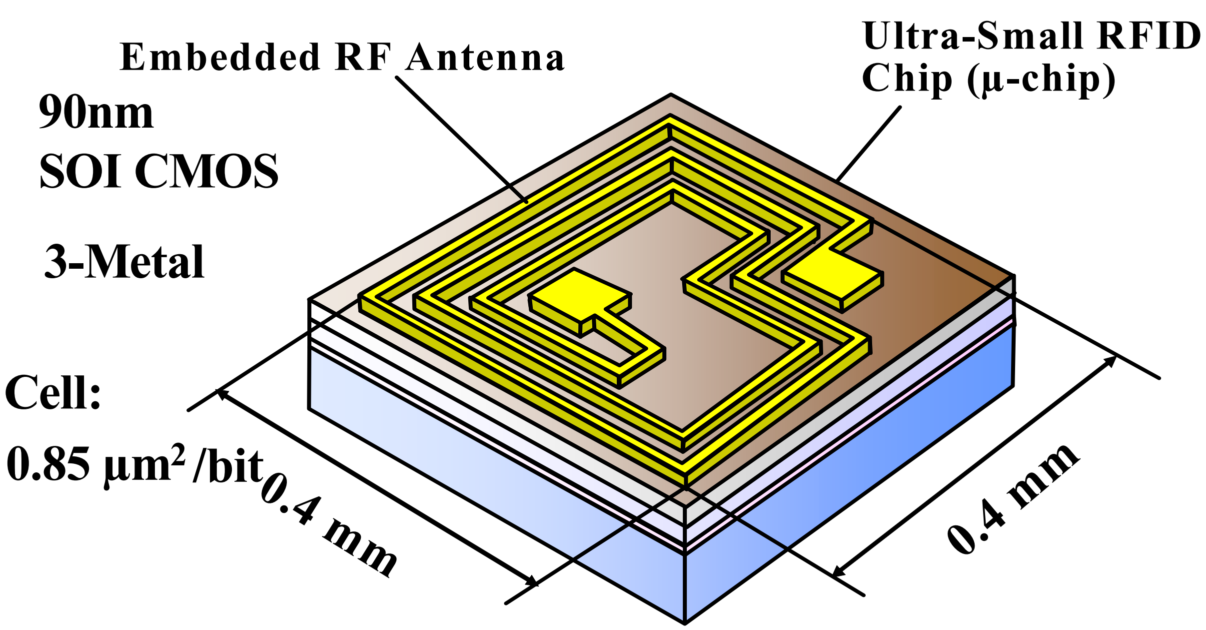

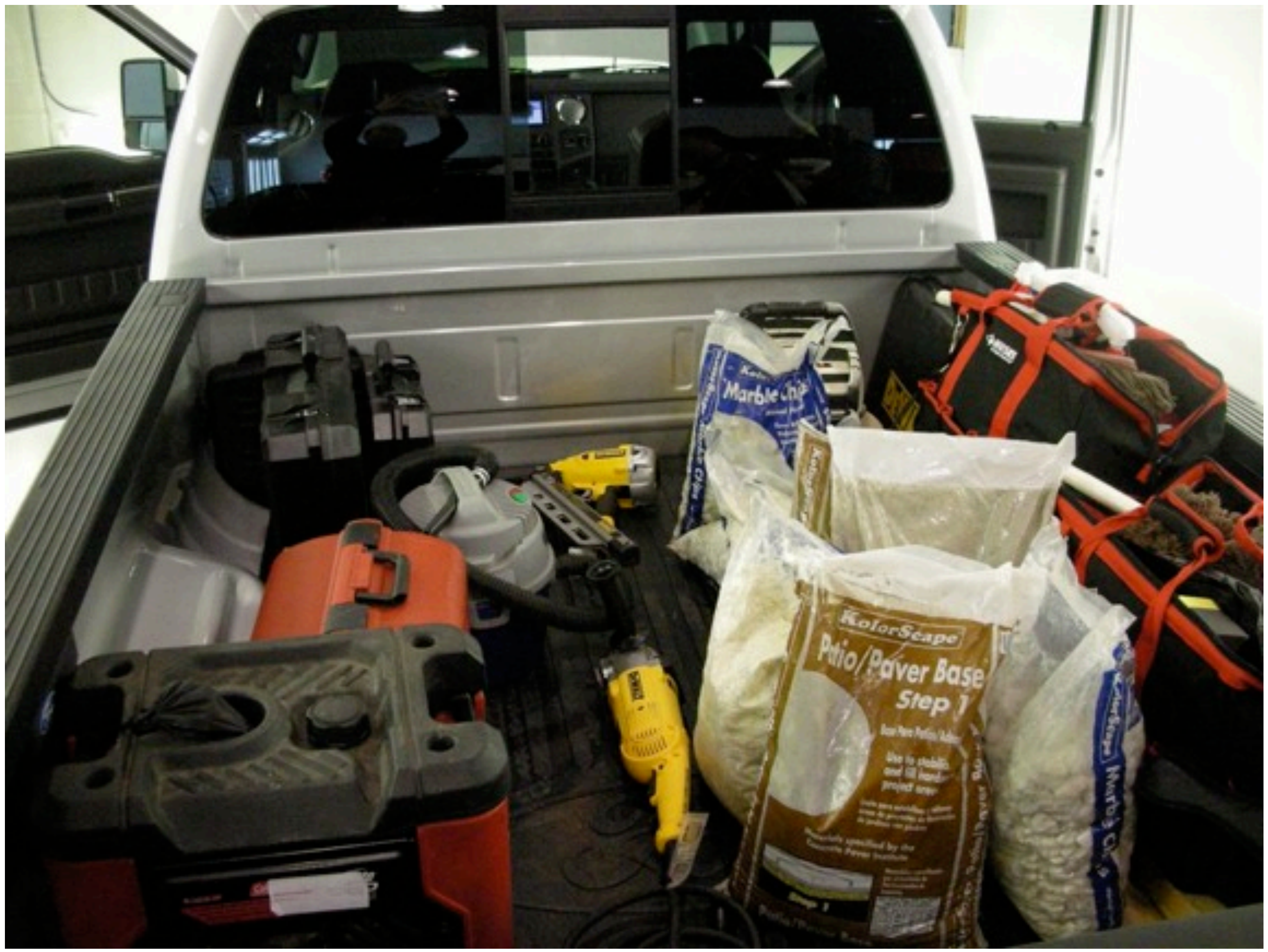
KolorScape
Patio/Paver Base
Step 1

Reality Engines

ThingMagic - Winner of 2008 Ford World Excellence Award

"Outstanding Feature" Award - Texas Auto Writers Association, Oct 2009

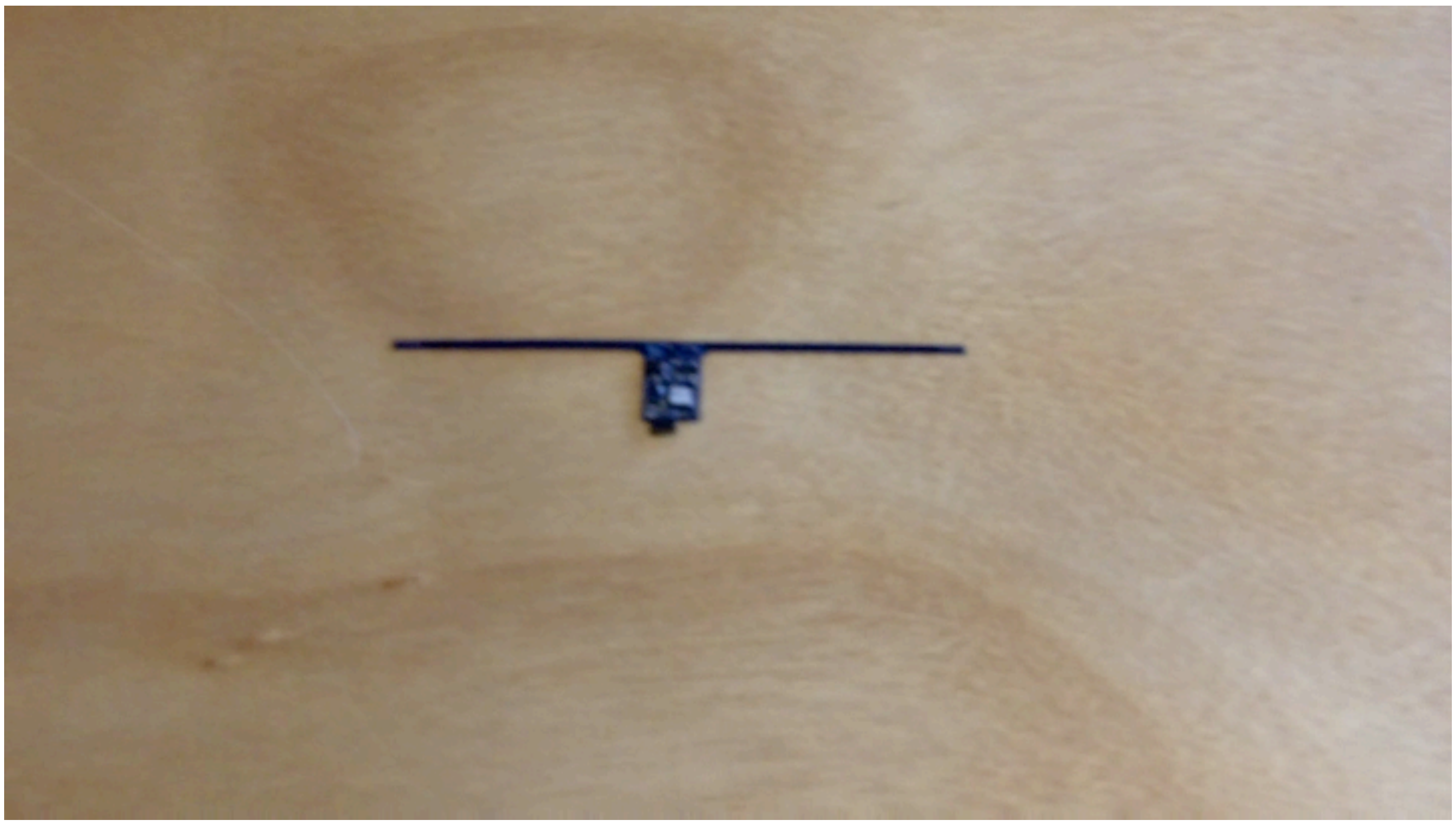

Polymerase = 7e+25 ops/kWh

Computing Efficiency

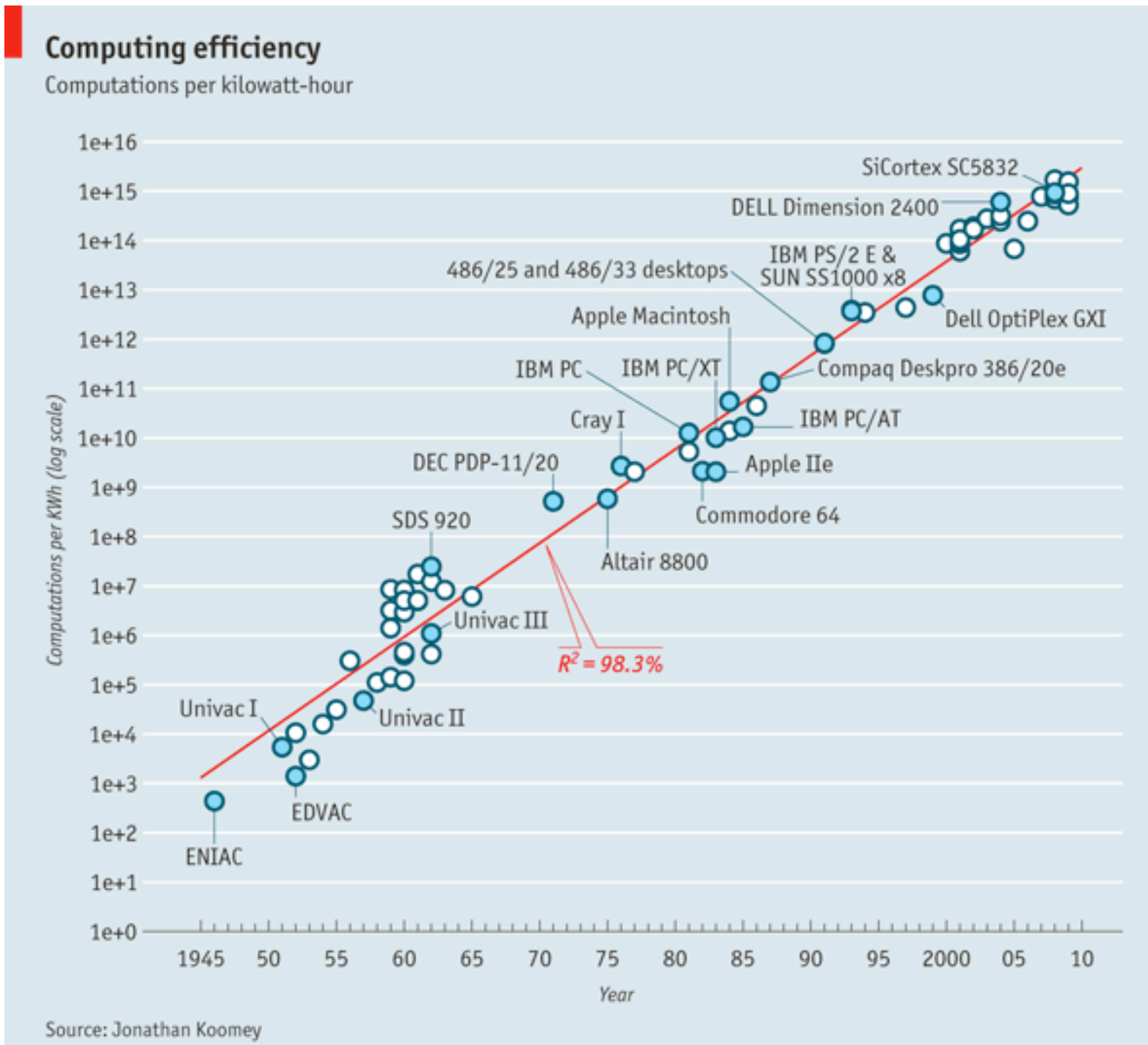

$$p(V) = \frac{e^{1/2CV^2/k_BT}}{\mathcal{Z}}$$

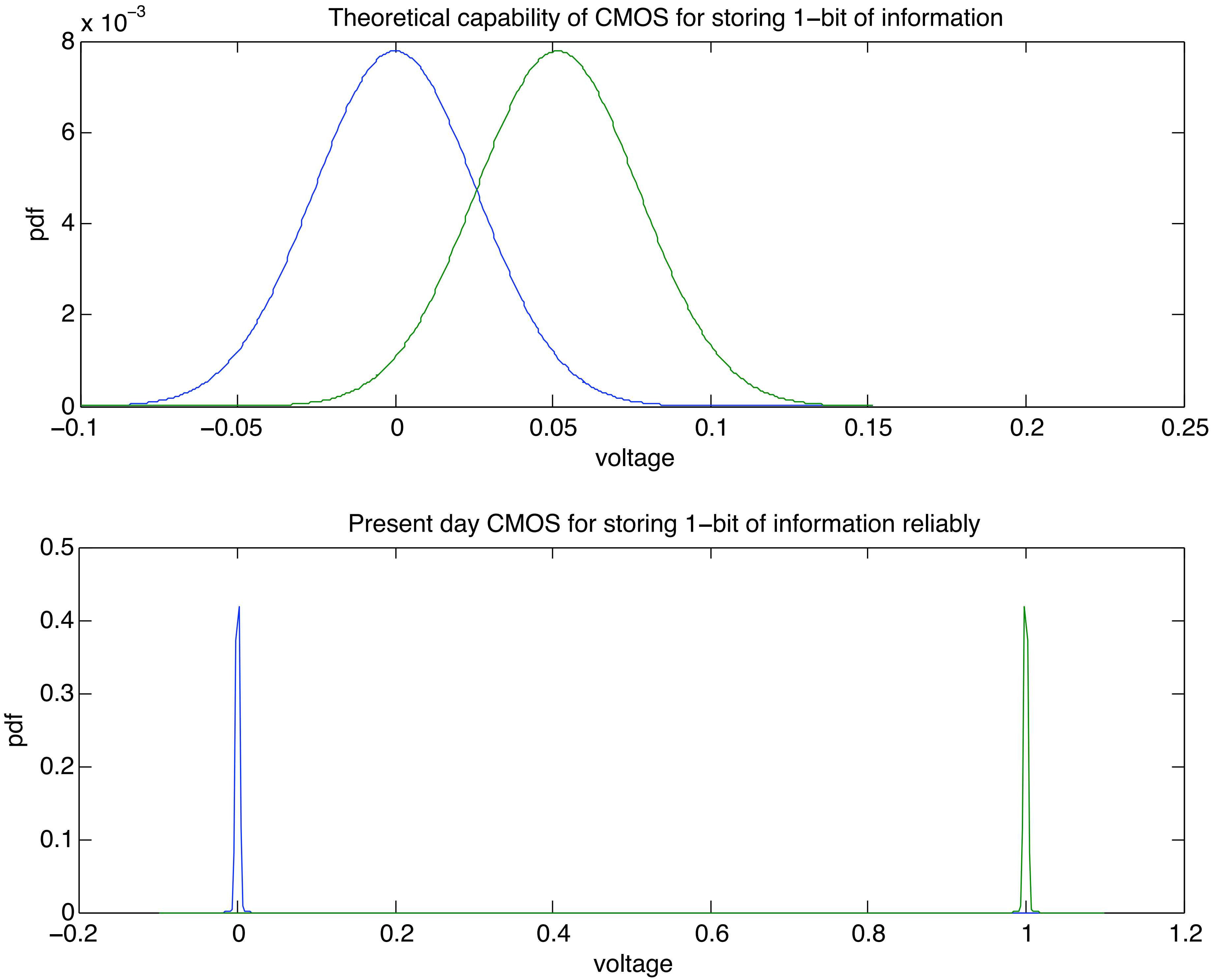

Challenge of Silicon

- Commercial RFID tag computes and communicates 128 bits at ~16-160 pJ/bit*
- Theoretical limit for information is kTlog(2)/bit or 2.9×10^{-21} J/bit or 1.4×10^{9} times lower
- DNA ligation is ~18x the limit*
- 2-3 orders of magnitude reduction of Si power could allow power from glucose

*

T. D. Schneider, J. Theor. Biol. 148,125 (1991)
R. C. Merkle, Nanotechnology4, 21 (1993)

Capacity and Noise Theorem

$$C_{\mathrm{awgn}} = \log_2(1 + SNR) \quad \text{bits/s/Hz}$$

$$\implies SNR_{\min} \geq 2^{C_{\mathrm{awgn}}} - 1$$

$$C_{\mathrm{awgn}} \times \mathrm{BW} = M \quad (10^{13} \quad \text{bits/s})$$

$$P_{\min} = SNR_{\mathrm{out}} + 10\log 10(k_B T) + 10\log 10 BW + NF + PL$$

Noise Spectroscopy in Brain

- Noise properties due to blood flow
- Carp et al, Biomedical Optics Express, 1 July 2011, V. 2 No. 7

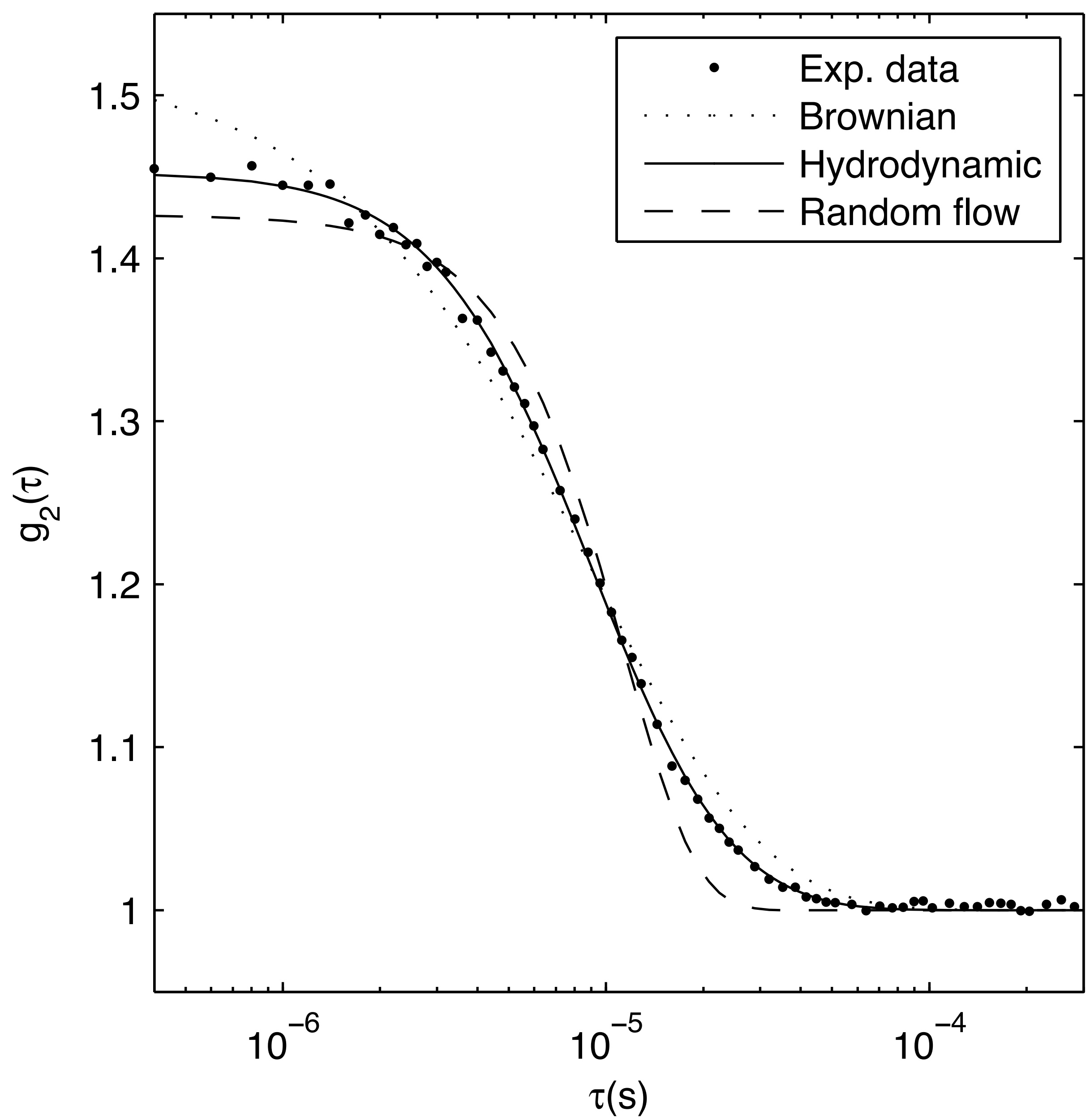

with 0 loss (800 nm = 3.75e14 Hz)...

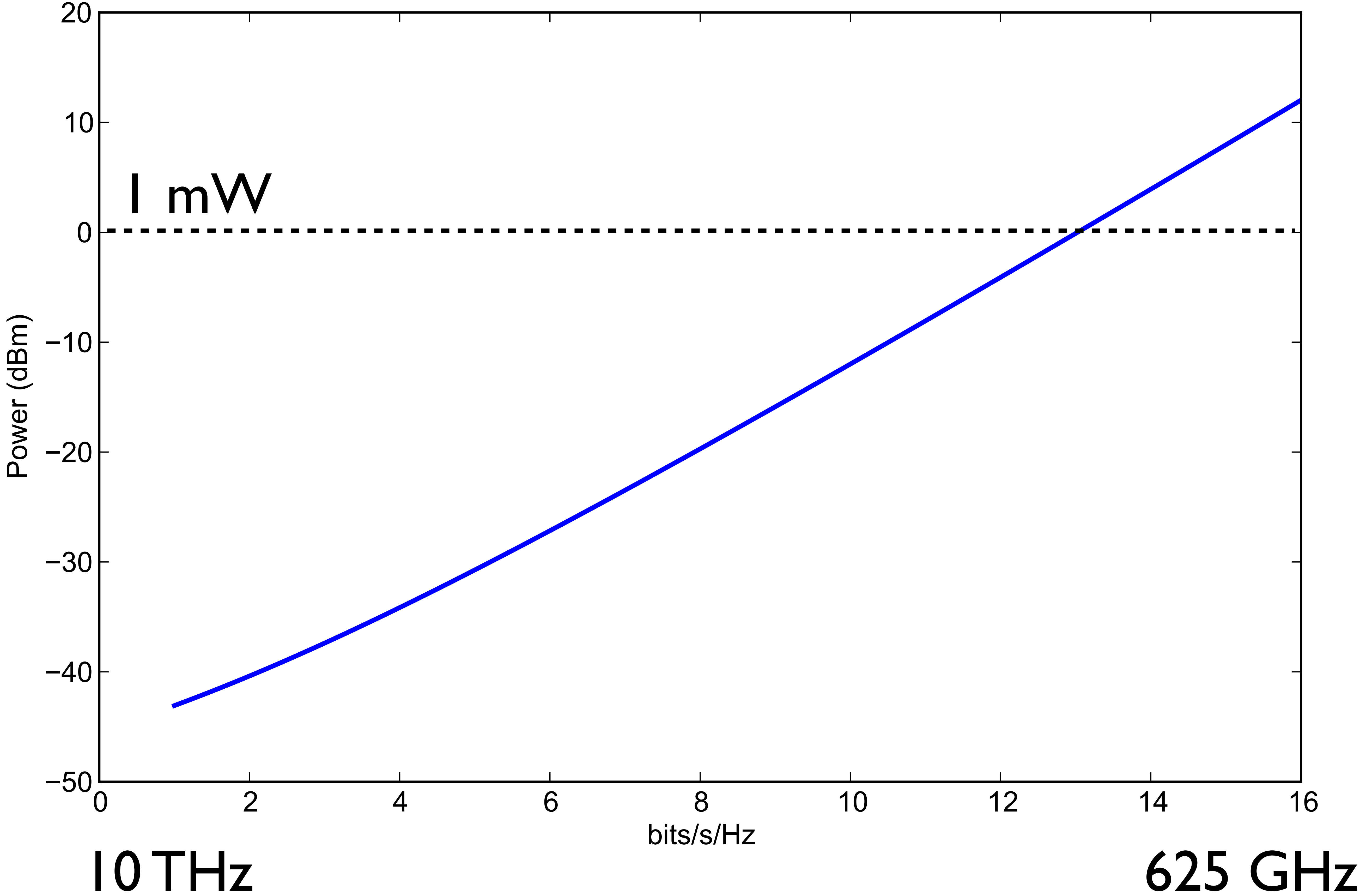

The Biological Absorption Window

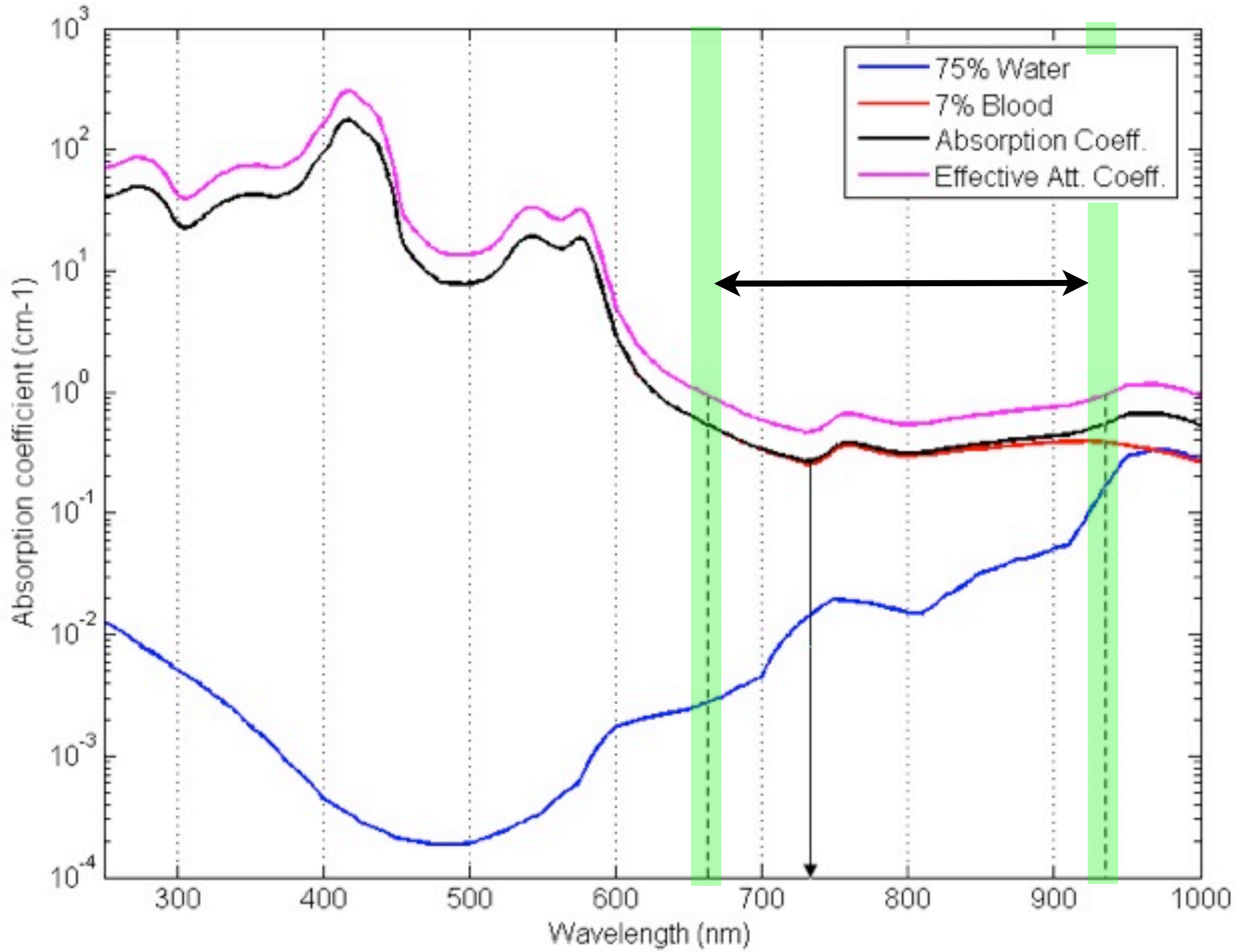

Utilize the photovoltaic effect in CMOS

- Goal: provide ~10 μW of DC power from external laser
- Challenge: 10 μW requires 8.3×10^5 W/m^2 (660 suns)
- M Ferri, D Pinna, and E Dallago. Integrated micro-solar cell structures for harvesting supplied microsystems in 0.35-μm CMOS technology. *Sensors*, Jan 2010 ⟶

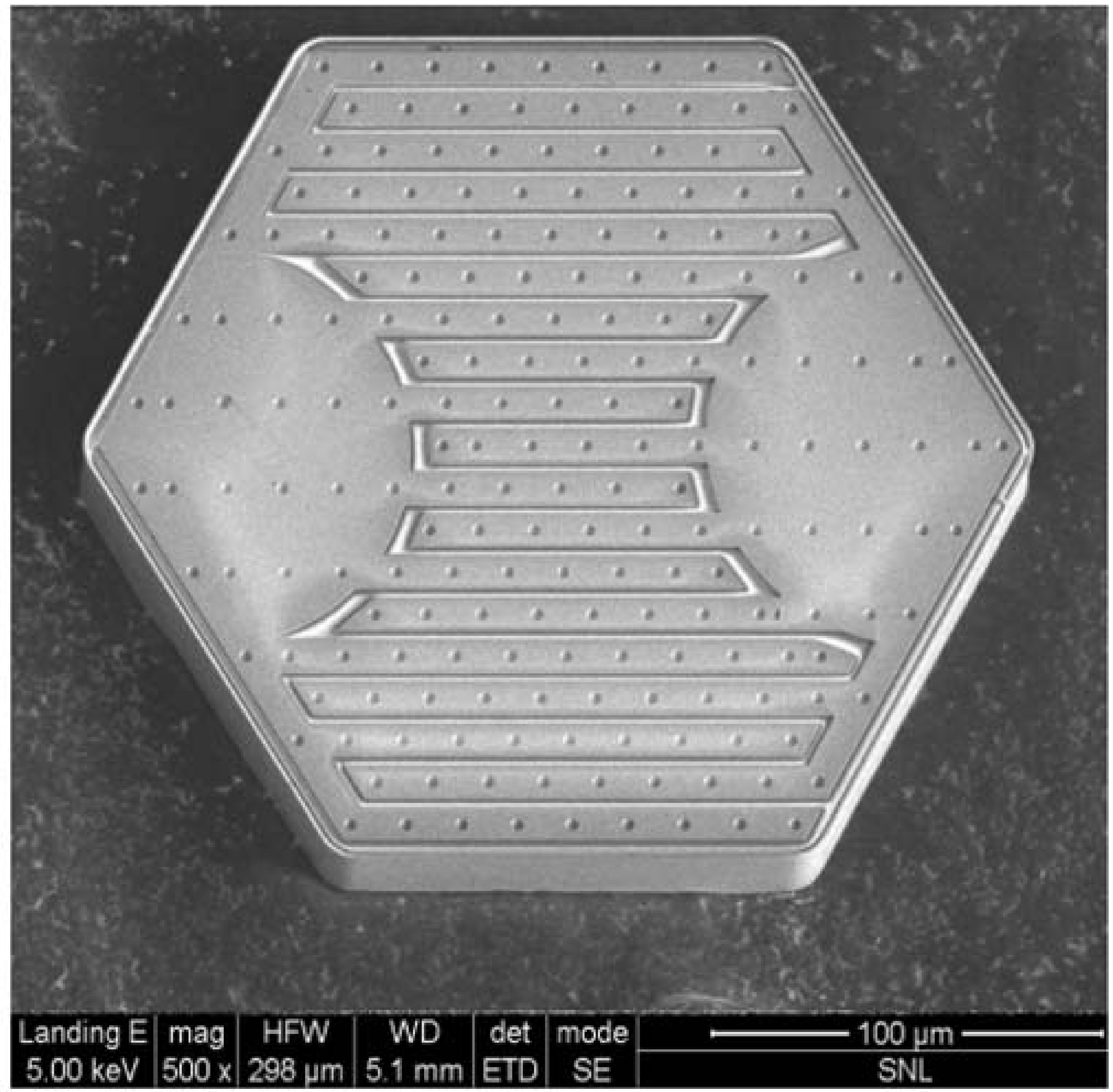

Modulation

- Change of radar-cross section (ΔΓ or DRCS)

$$P_{\text{total}} = P_{\text{load}} + P_{\text{scatter}}$$

- Tag dynamically changing load impedance = data

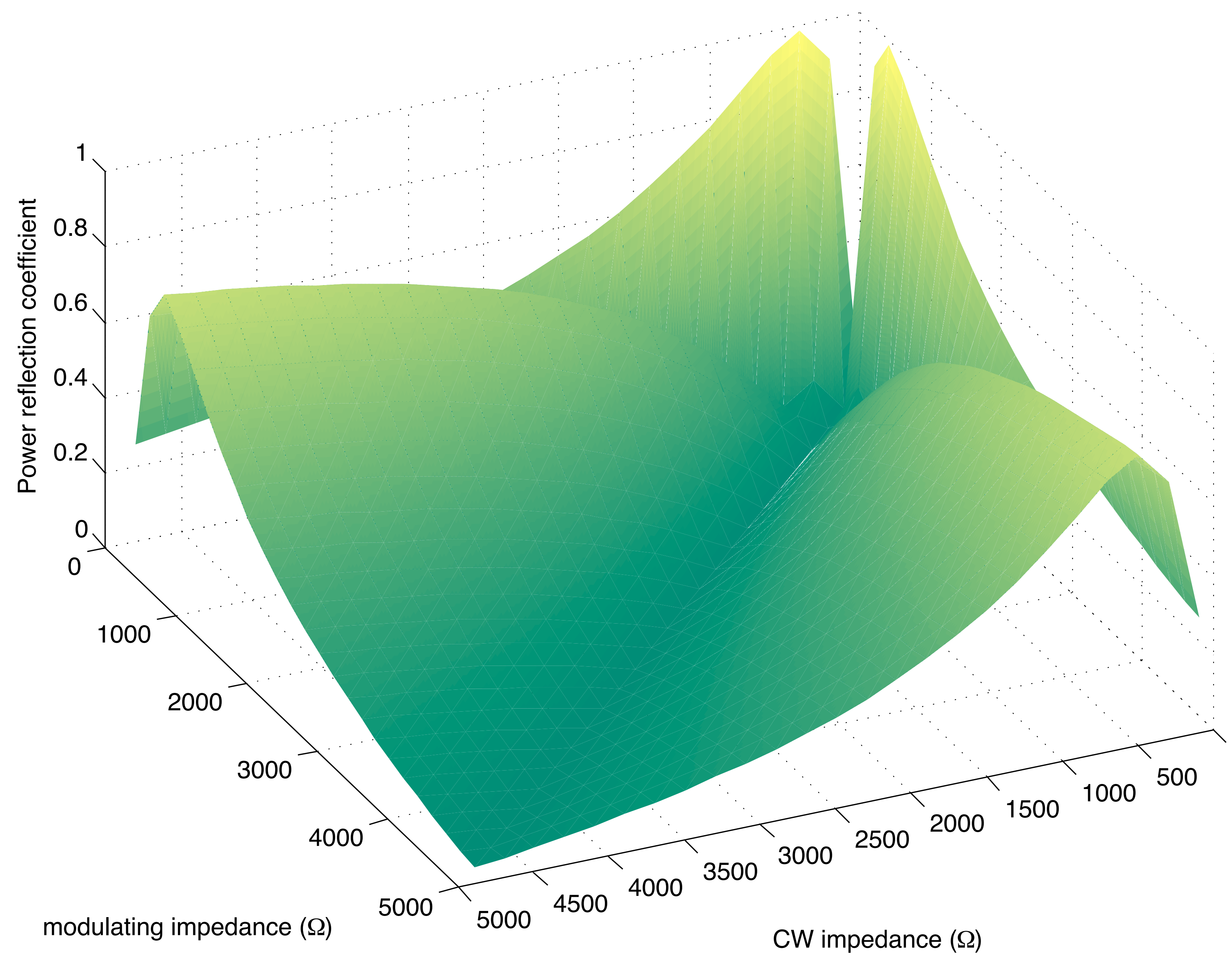

C Nanotube radio

Rutherglen and Burke, Carbon Nanotube Radio, Nano Letters, v. 7, No. 11, 2007

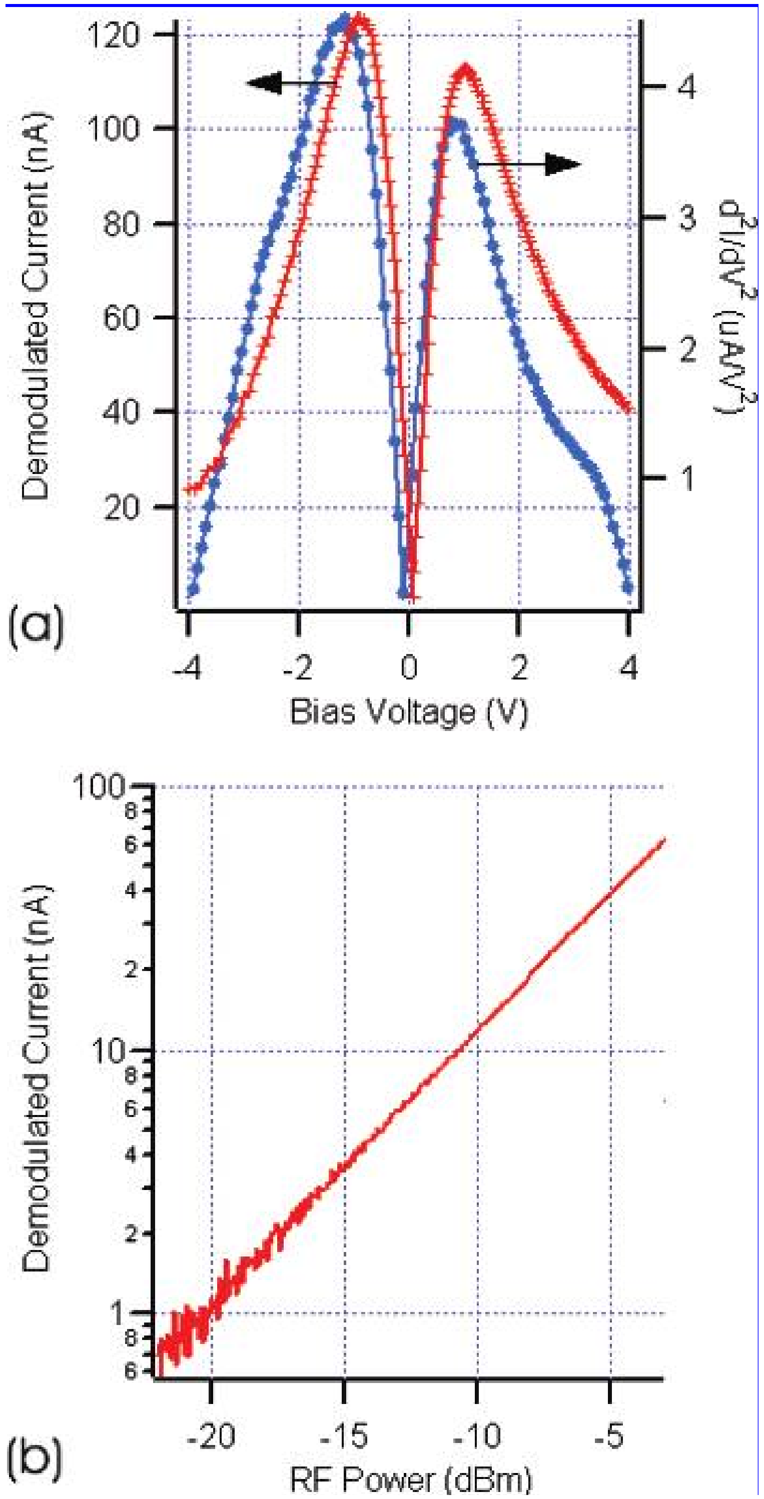

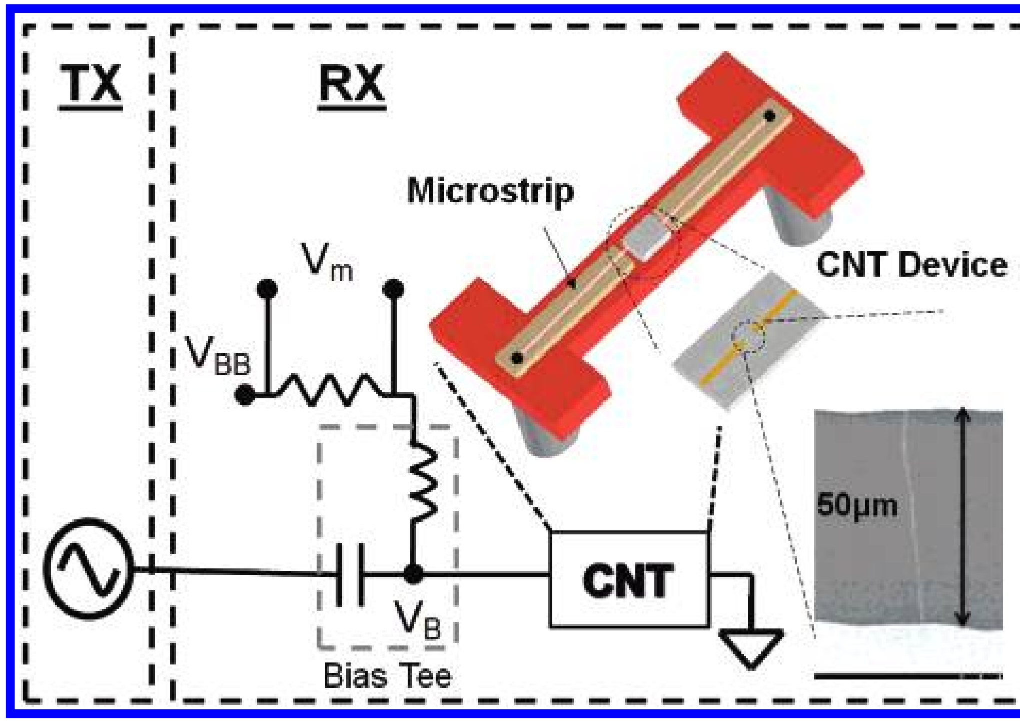

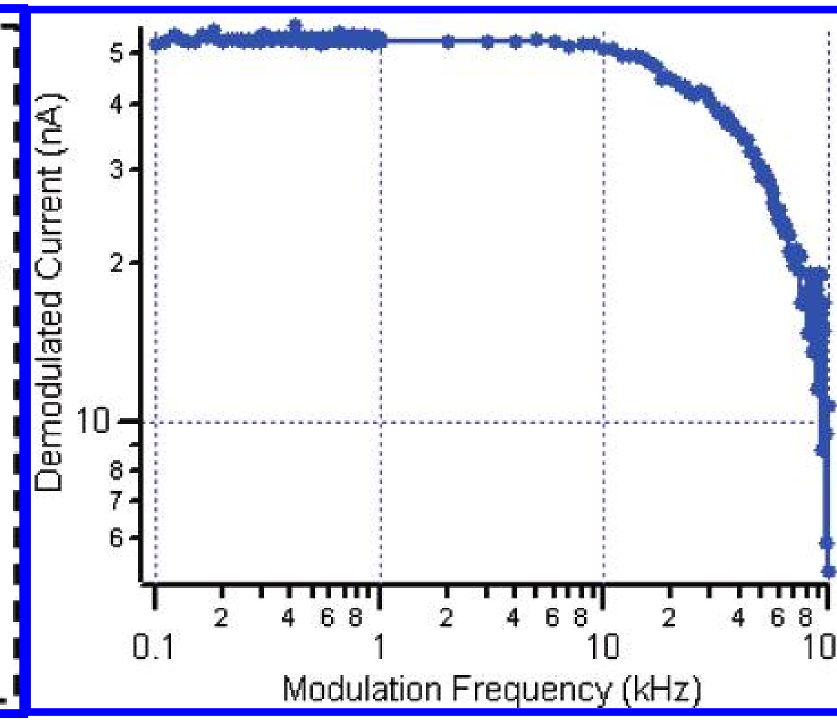

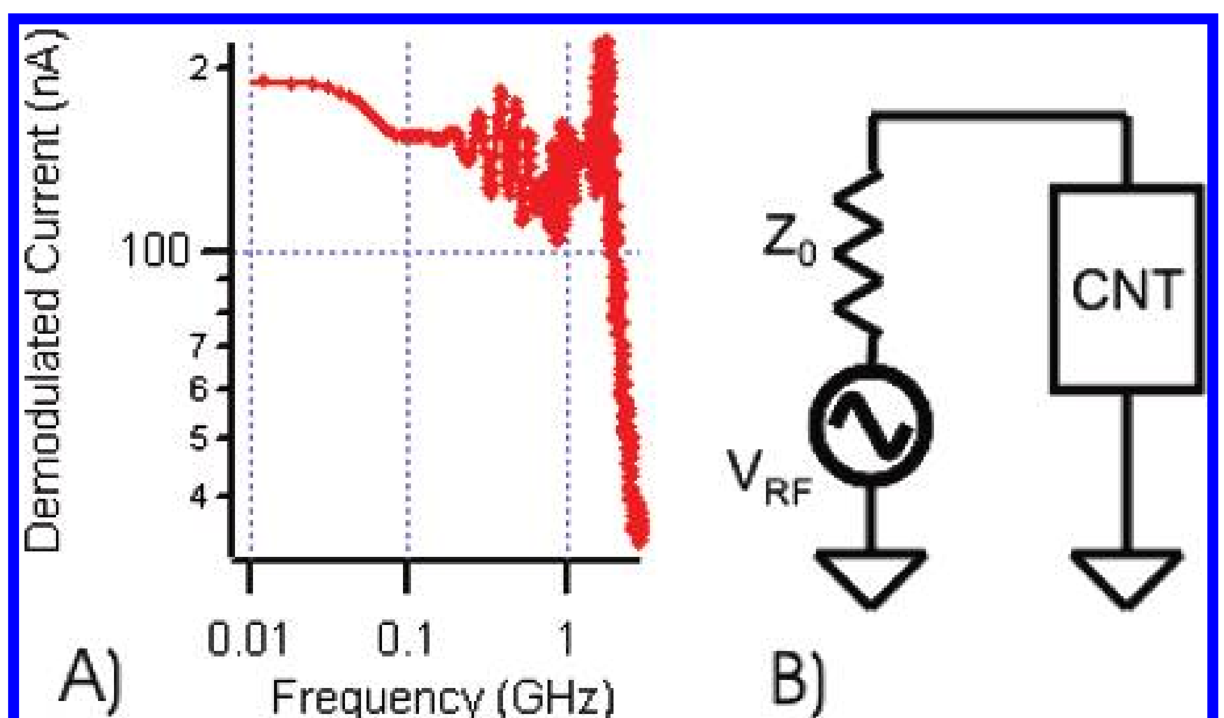

Backscatter

- Reflectance of material is dynamically changed digitally
- Liquid crystals operate with >95% efficiency
  - Ravi K. Komanduri, Chulwoo Oh, and Michael J. Escuti. Reflective liquid crystal polarization gratings with high efficiency and small pitch (proceedings paper). *Liquid Crystals XII*, 7050, Jan 2008
- May need new fabrication techniques for optical components at this scale
  - iPhone 5 pixel is 78 µm
  - Smallest DLP microdisplay pixel is 5 µm

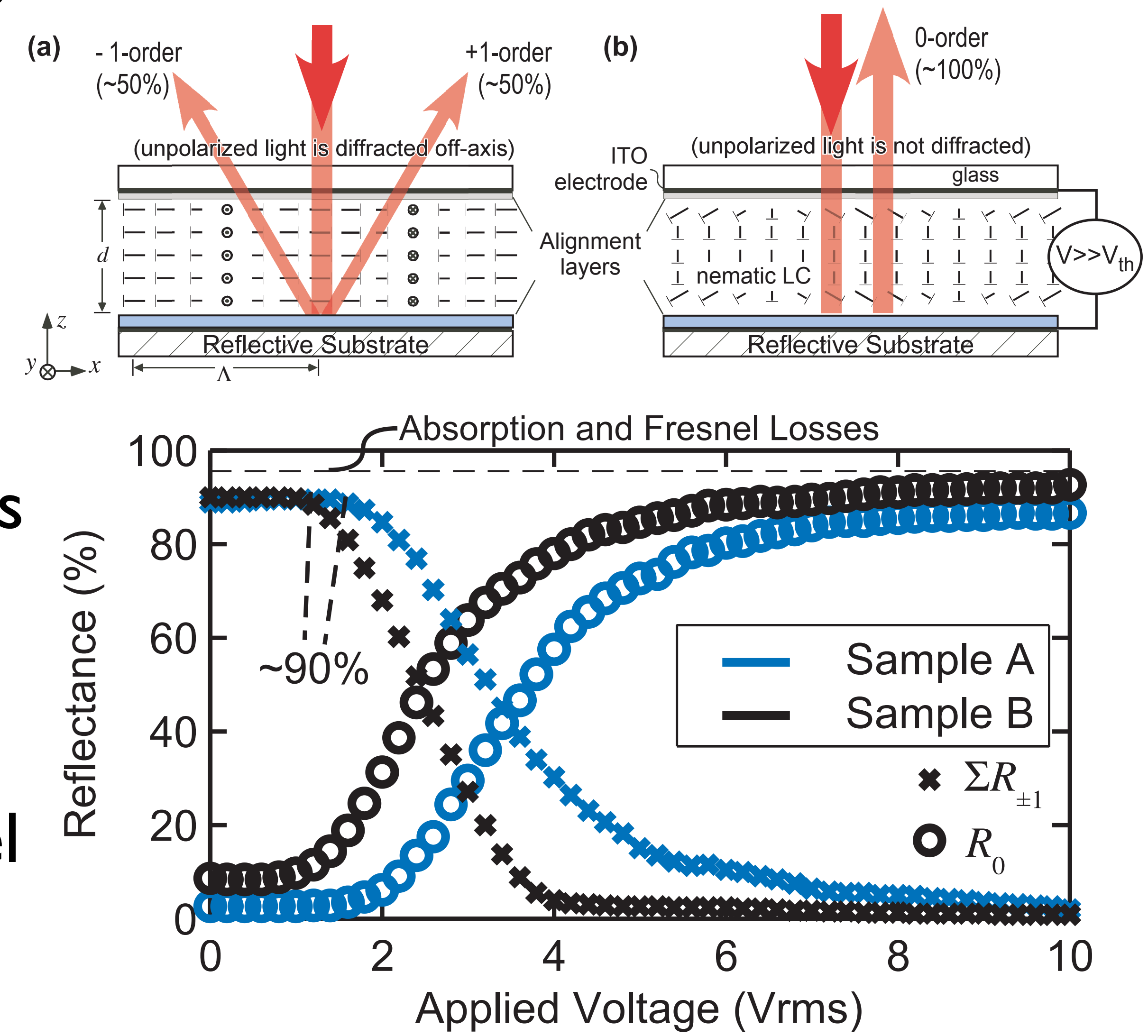

Reverse Link Channel

- Hypothesis: mesoscopic scattering in tissue is an optical amplifier above body noise of 100kHz
    - Richard Berkovits. Sensitivity of the multiple-scattering speckle pattern to the motion of a single scatterer. *Physical Review B*, 43(10):1–3, Apr 1991

$$\lambda \ll l \ll L \ll L_{\mathrm{coherence}}$$

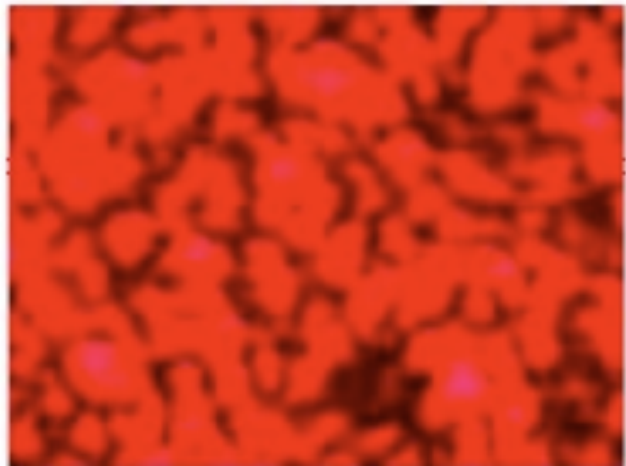

Speckle Interferometry as a Sensor

- Coherent waves propagating through a disordered structure produce speckle patterns.
  - Speckle patterns are extremely sensitive to changes in the structure and can be used to robustly detect very small changes to the structure.
  - Given that the binding of an odorant molecule to an OR causes a conformational change in the structure, this change can be detected by looking at correlations between speckle patterns or statistics derived from them.
  - Prior work enabling this approach includes:
    - Berkovits, Phys. Rev. B, 43, 10, 1991.
    - Pappu et. al., Science, 297, 2001:

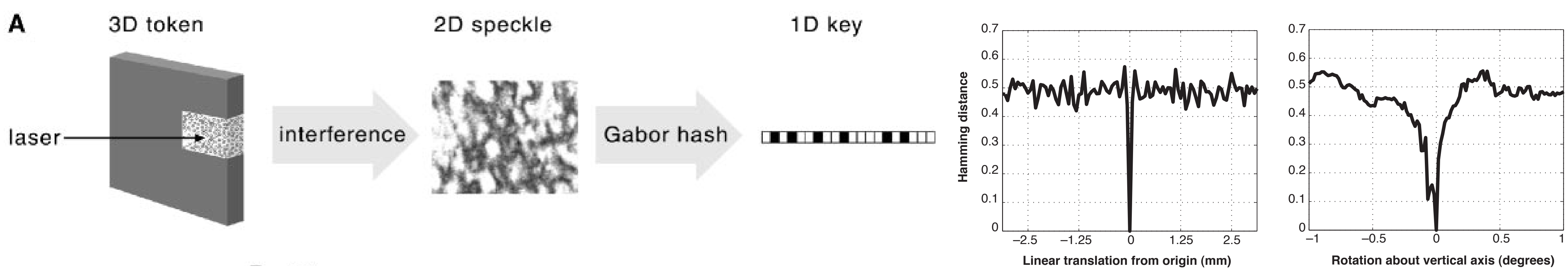

Length scales

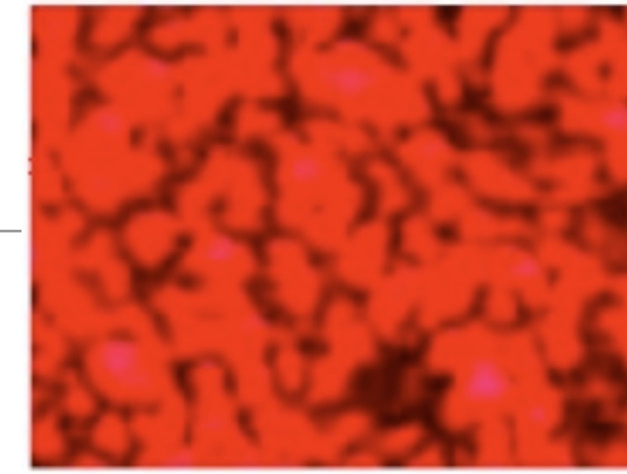

- Coherent multiple scattering occurs when

$$\lambda \ll l \ll L \ll L_{coherence}$$

where λ is the wavelength of the probe, l is the mean-free path between scattering centers (i.e., odorant-OR bonds or cells in the brain), L is the thickness of the structure, and $L_{coh.}$ is the coherence length of the probe.

- Single scattering occurs when:

$$\lambda \ll L \ll l$$

- In this case the probe beam interacts with a single scattering center before exiting the sample

Sensitivity of speckle pattern

- The speckle pattern decorrelates completely when more than $A/(Ll)$ scatterers are moved (or new bonds are created) or if the probe beam angle changes by more than $\lambda/(2\pi L)$
- This decorrelation sets an upper bound on the odorant concentration and sample size.

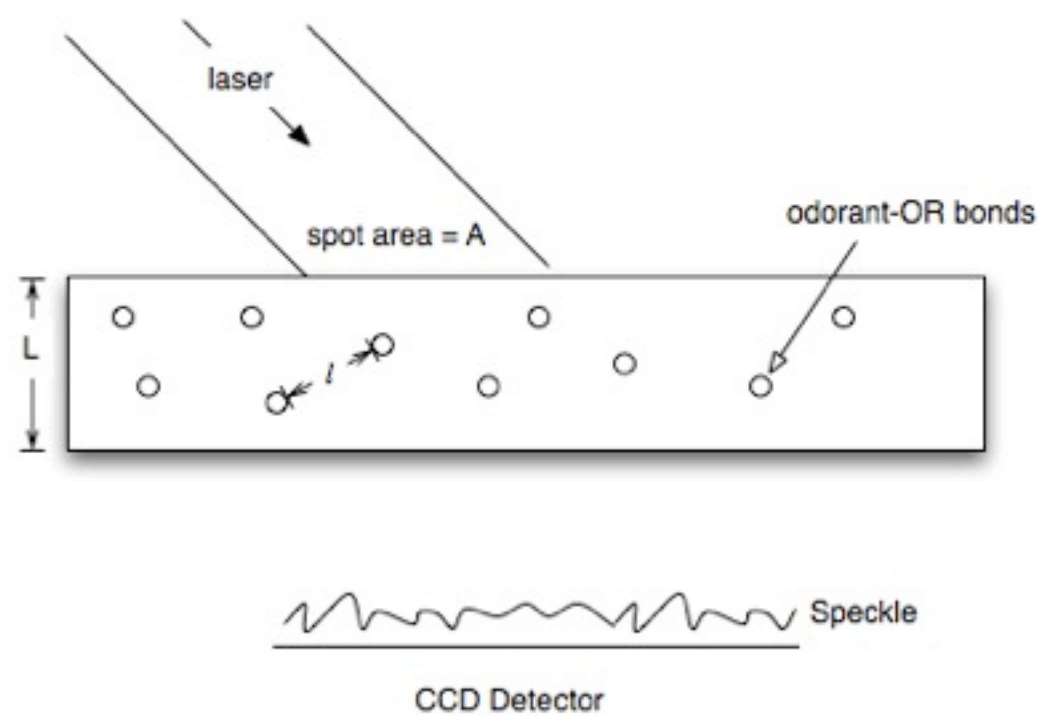

Test apparatus

- The following test apparatus was built to characterize the various length scales and determine the eventual sensitivity of the speckle to the concentration of odorant-OR bonds

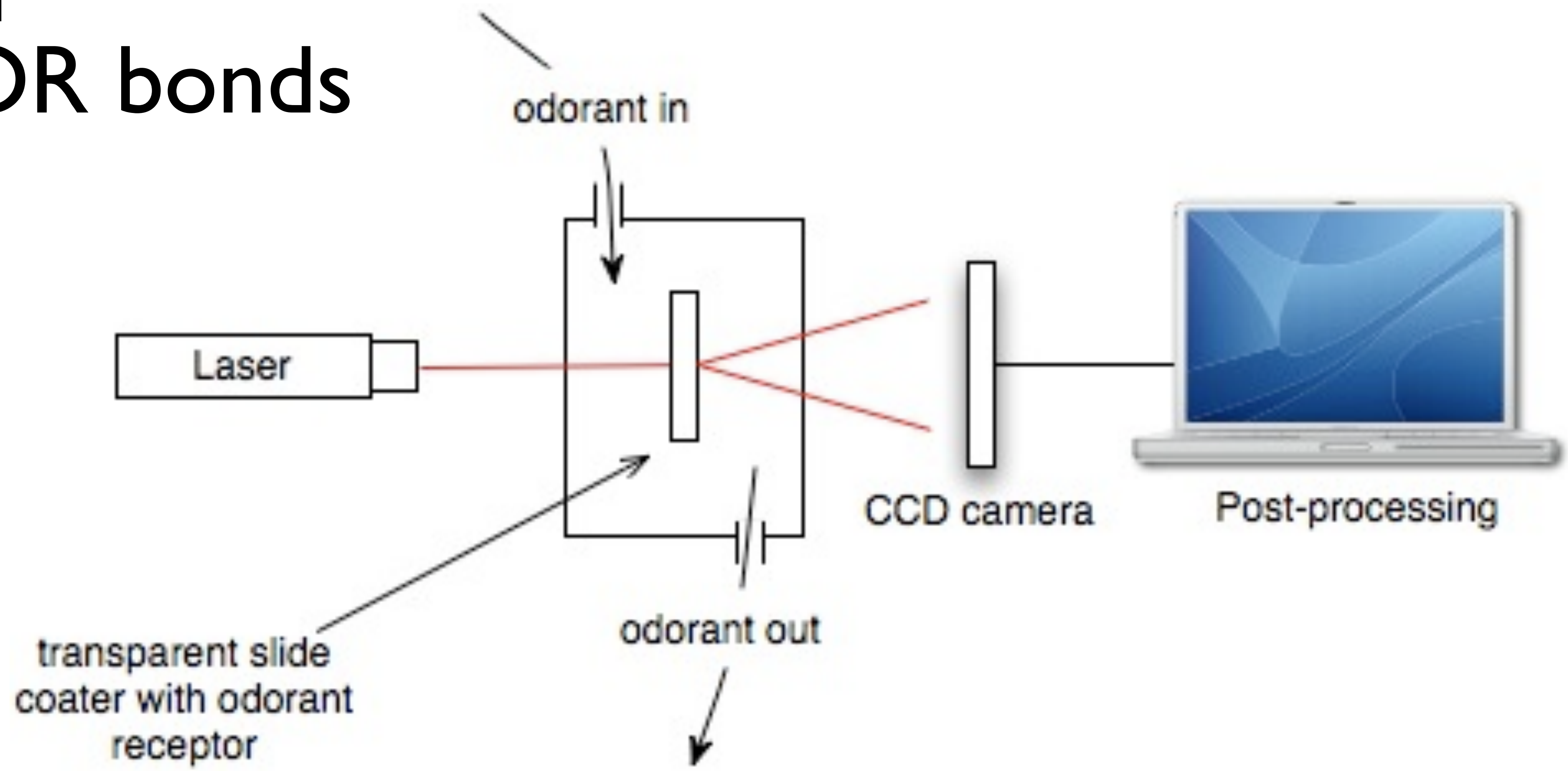

Test Apparatus

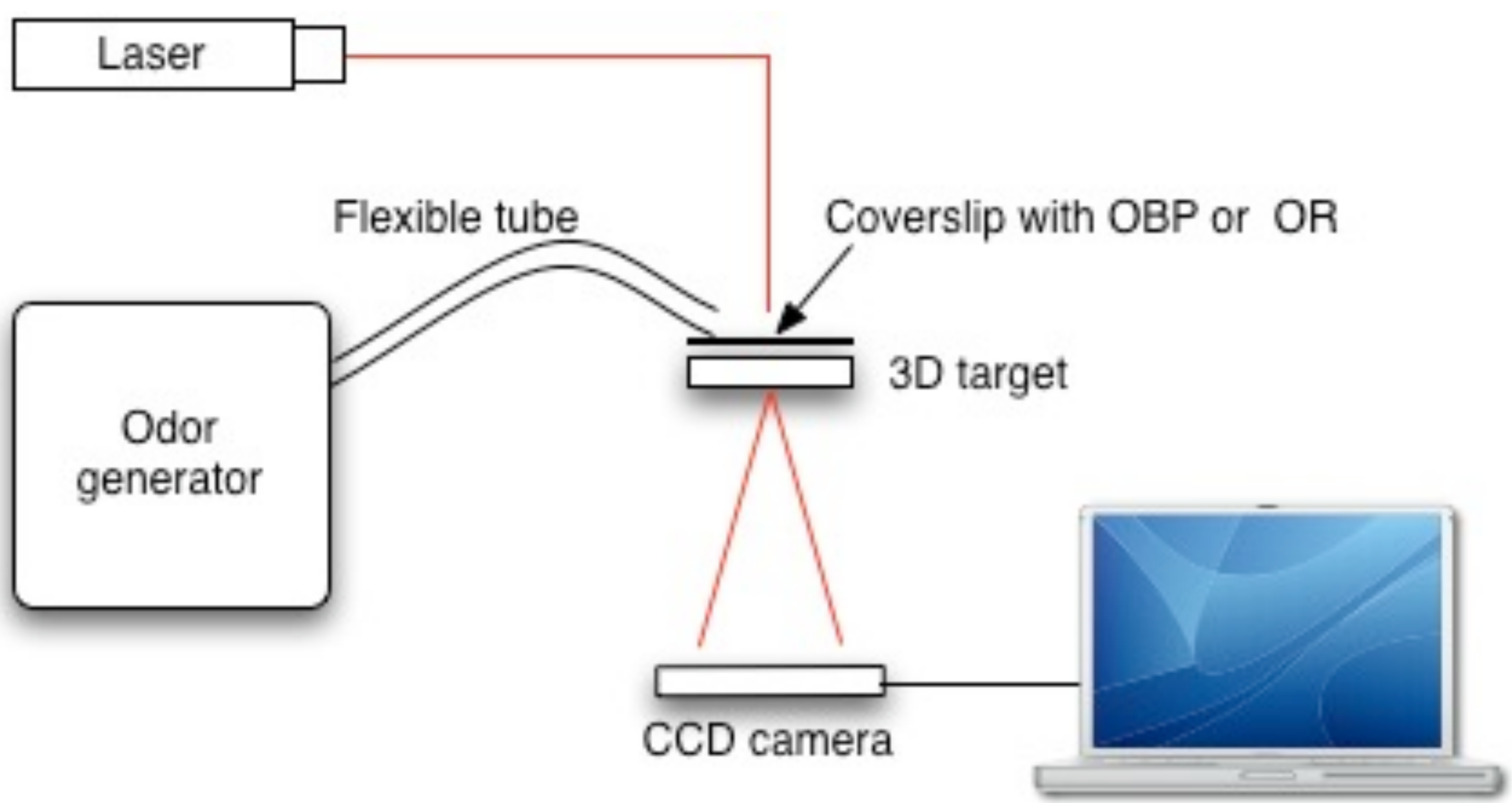

Test Apparatus

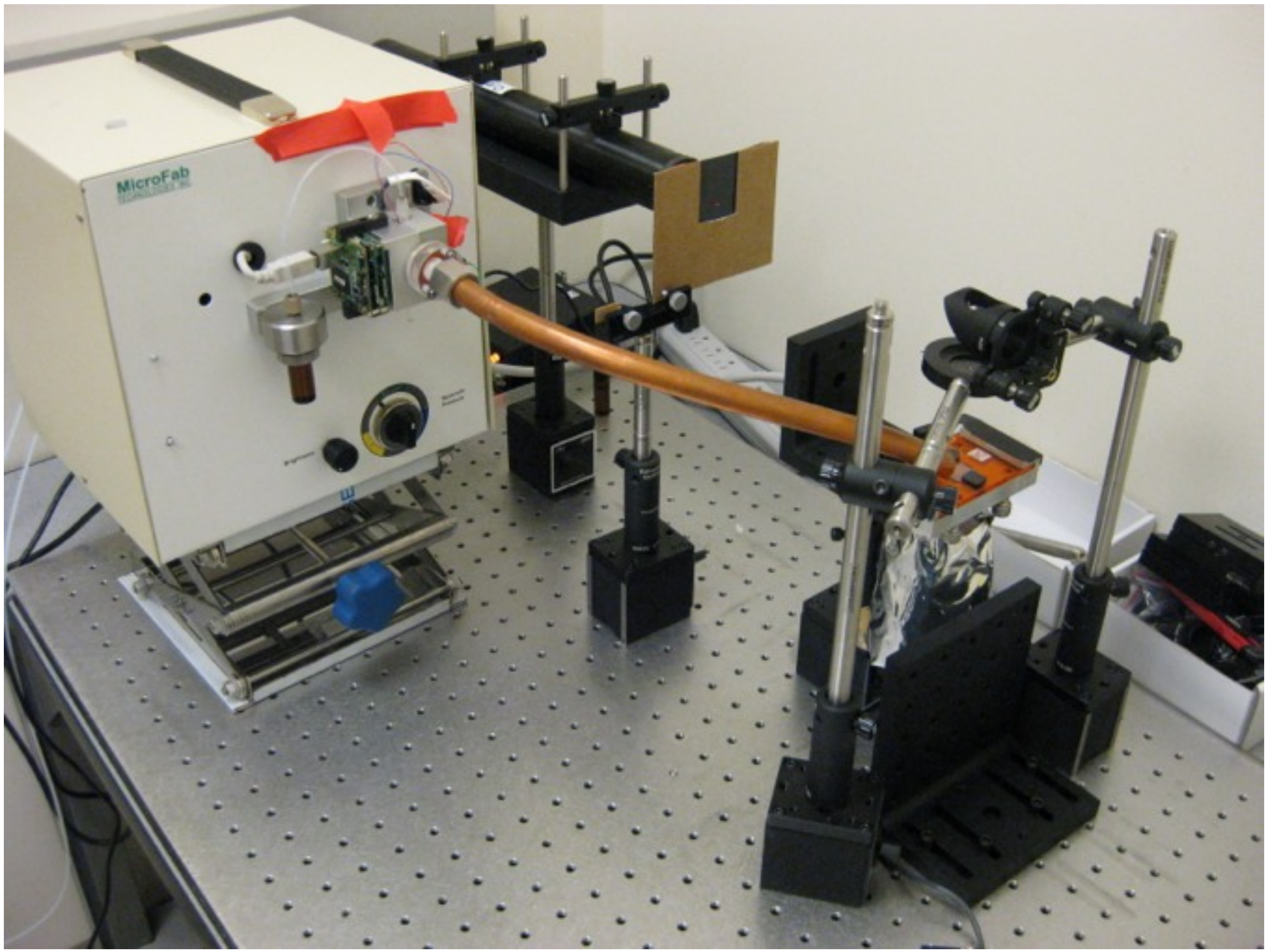

Final Setup of Speckle

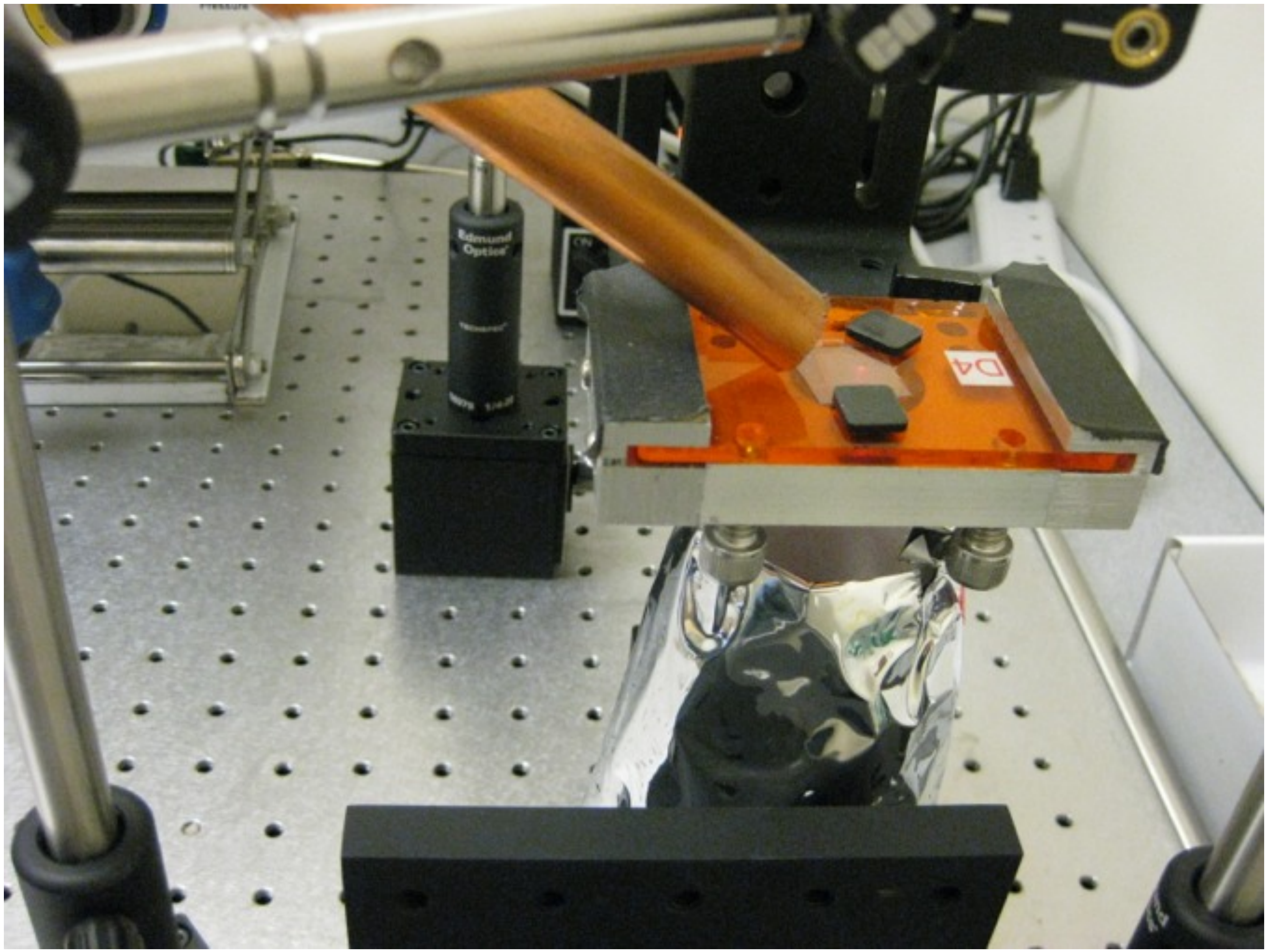

OR Construction Status (Zhang Lab)

OR #	OR Name	Mamalian		Wheat Germ		E. Coli	
		Inserted	Seq.	Inserted	Seq.	Inserted	Seq.
1	mOR106-13 (S3)	✔	✔	✔	✔	✔	✔
2	mOR175-1 (OR912-93)	✔	✔	✔	✔	✔	✔
3	hOR17-209 (OR1G1)	✔	✔	✔	✔	✔	✔
4	mOR33-1 (S19)	✔	✔	✔	✔	✔	✔
5	hOR17-210 (OR1E3)	✔	✔	✔	✔	✔	✔
6	mOR171-2 (M71)	✔	✔	✔	✔	✔	✔
7	mOR103-15 (I7)	✔	✔	✔	✔	✔	✔
8	mOR276-1 (G7)	✔	✔	✔	✔	✔	✔
9	mOR31-4	✔	✔	✔	✔	✔	✔
10	mOR174-4 (EV, OR74)	✔	✔	✔	✔	✔	✔
11	mOR174-9 (EG, OR73)	✔	✔	✔	✔	✔	✔
12	OLfr226-17 (rat)	✔	✔	✔	✔	✔	✔

- All 36 expression constructs complete
- Plasmids verified by DNA sequencing

E. Coli Cell-Free Synthesis

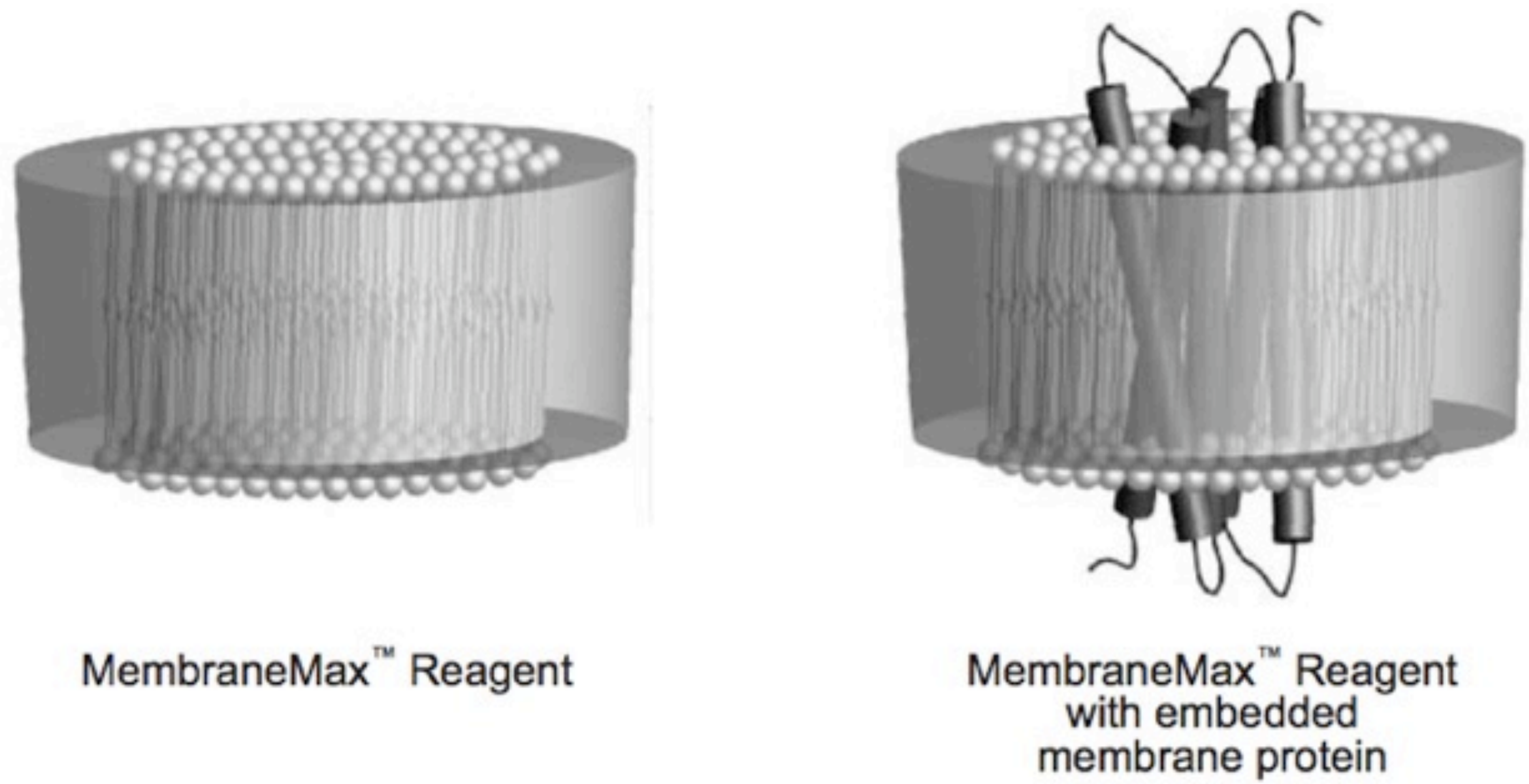

Initially we tested an E. coli-based cell-free synthesis of OR using MembraneMax (Invitrogen).

MembraneMax reagent is a nanolipoprotein complex consisting of a scaffold protein ring surrounding a planar DMPC lipid bilayer. Synthesized membrane proteins (such as an OR) become embedded in the MembraneMax reagent, which mimics the natural cellular environment (Invitrogen).

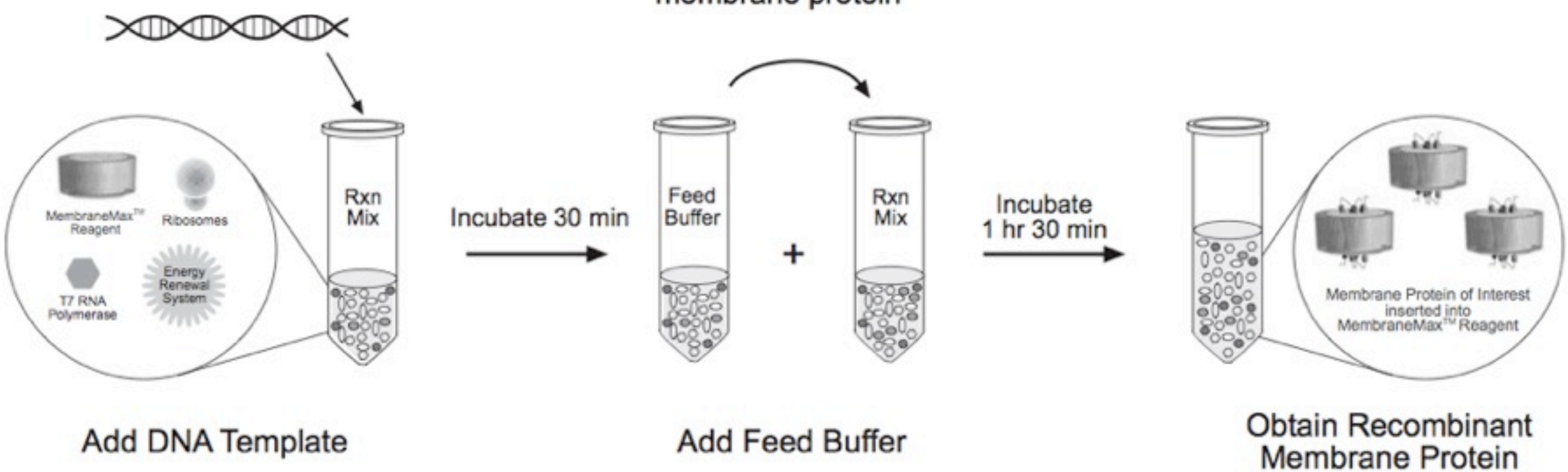

Speckle Response

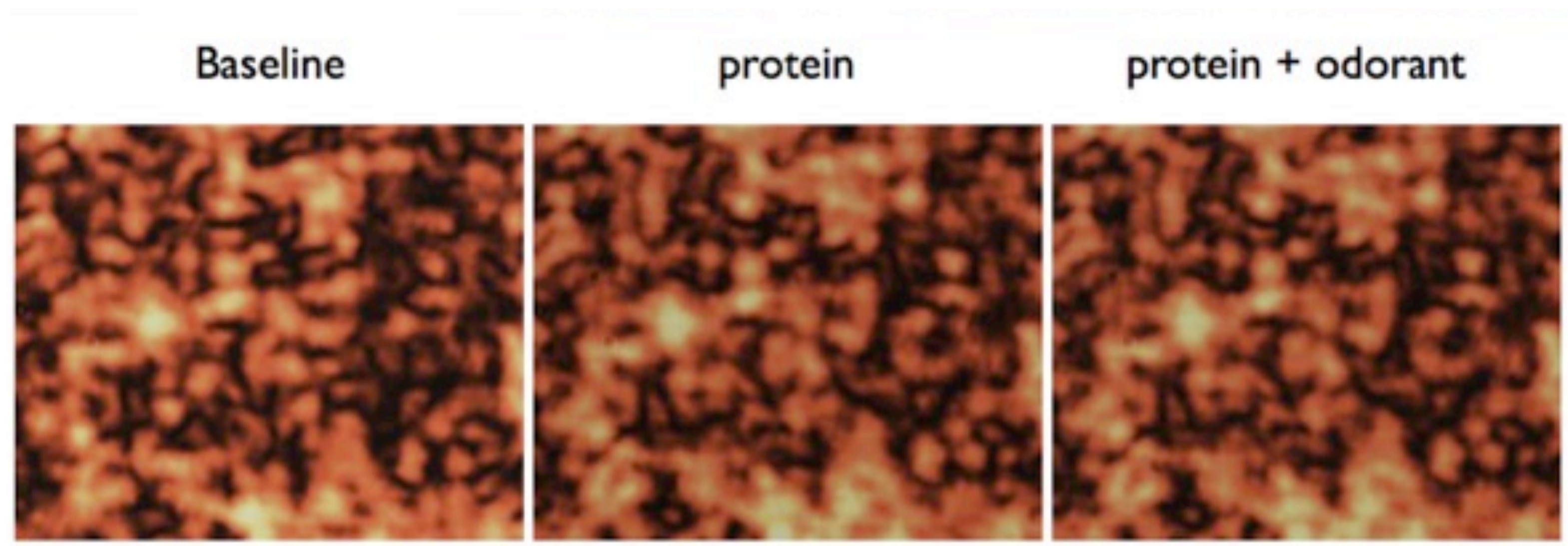

Speckle Results

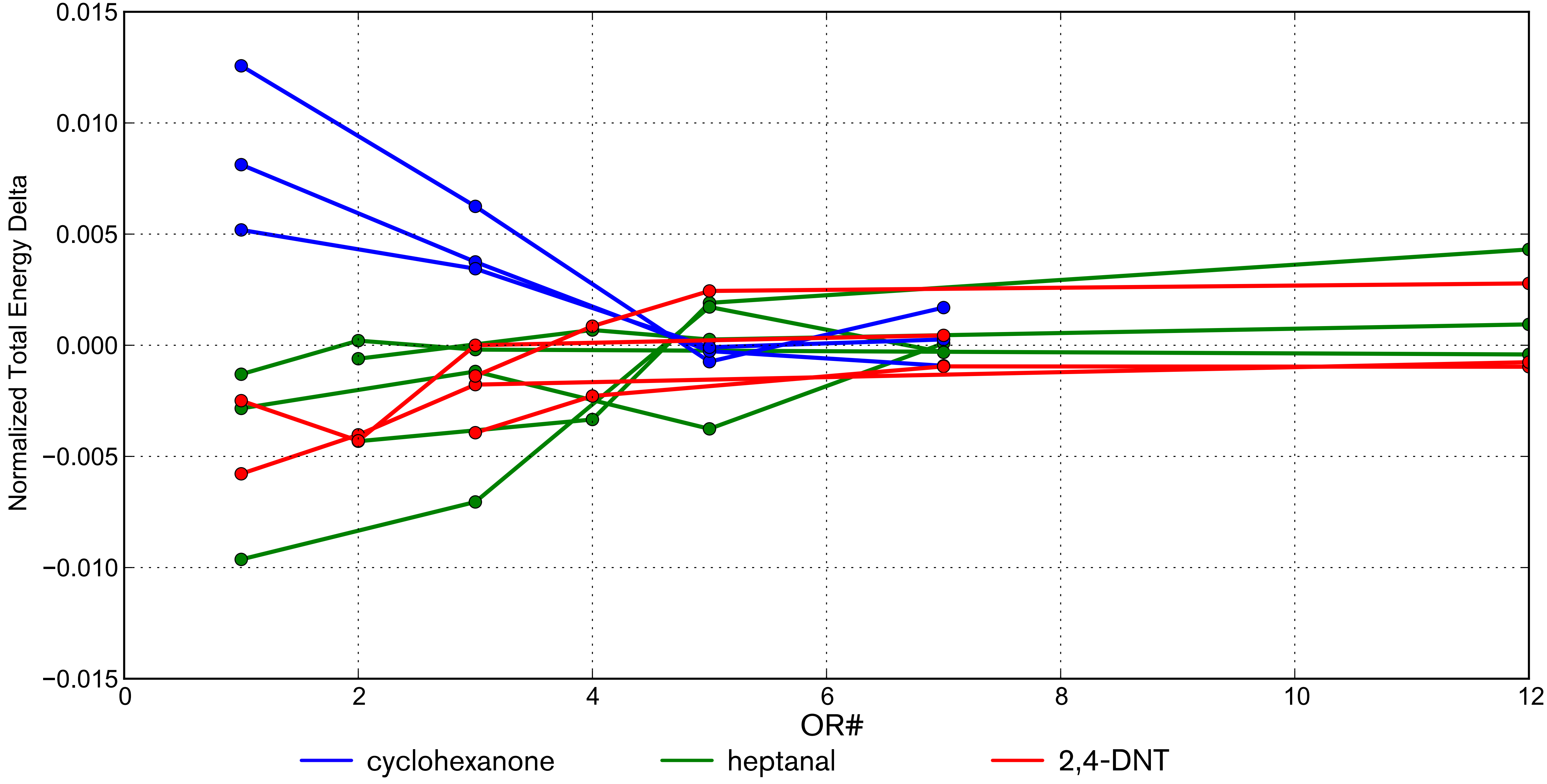

Results

- overall ~70% success in identifying 3 different odorants and low to high concentration (few ppB to 10s of ppB)

- more difficult detecting higher concentrations of odorants than lower concentrations

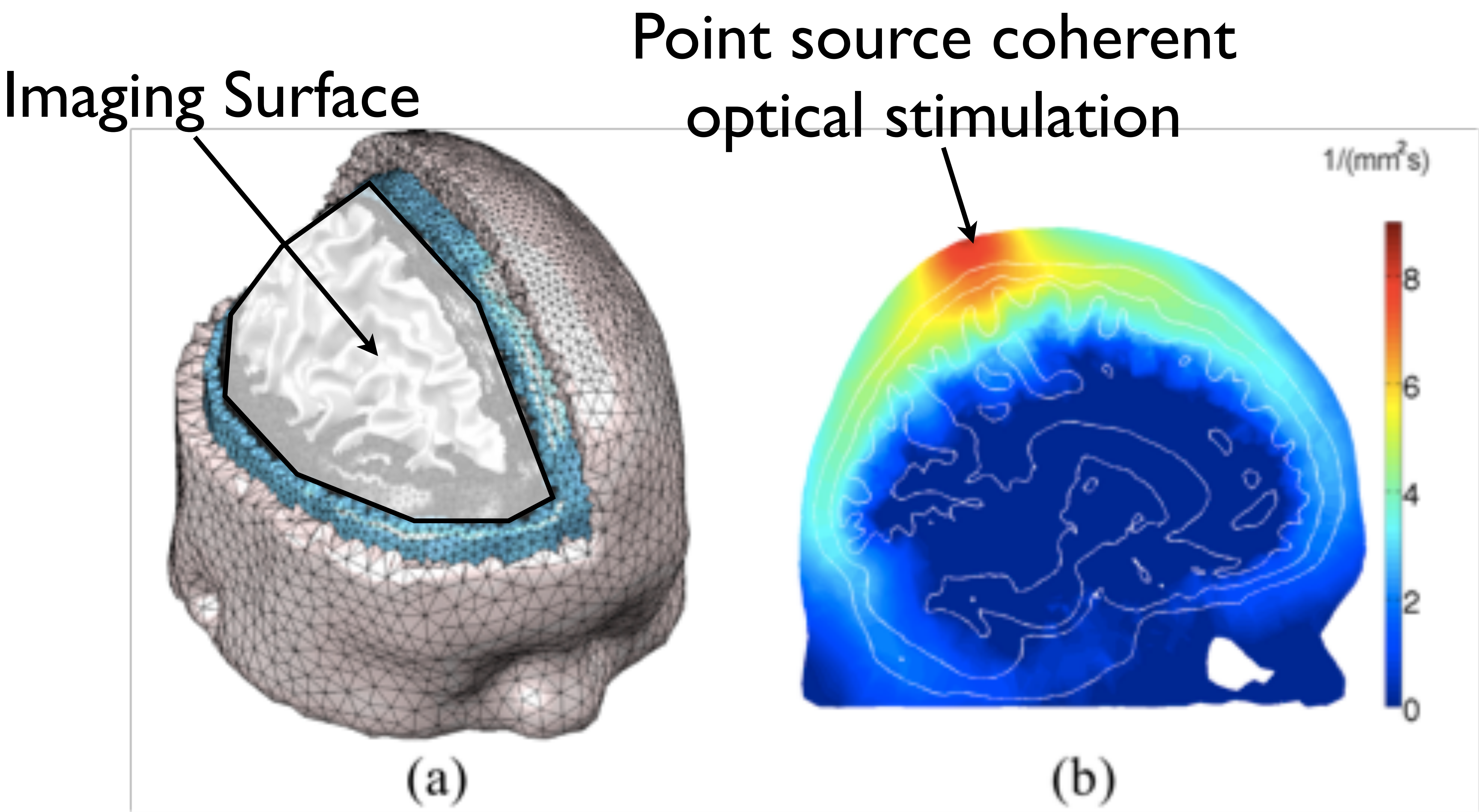
Imaging Surface
Point source coherent optical stimulation
1/(mm²s)
8
6
4
2
0
(a)
(b)

Schematic

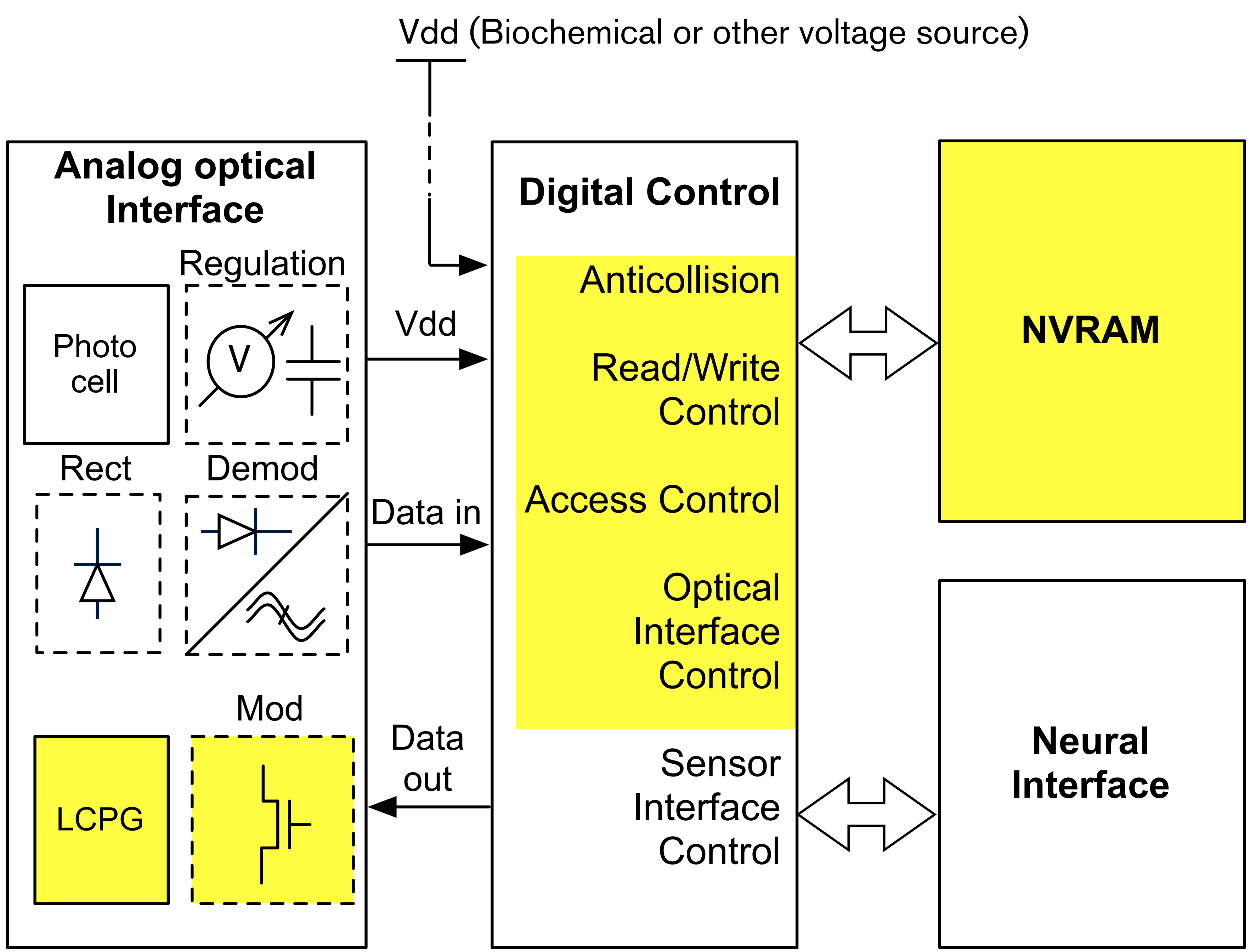
Vdd (Biochemical or other voltage source)
Analog optical Interface
Regulation
Photo cell
V
Rect
Demod
Mod
LCPG
Vdd
Data in
Data out
Digital Control
Anticollision
Read/Write Control
Access Control
Optical Interface Control
Sensor Interface Control
NVRAM
Neural Interface

Design (dual-sided*)

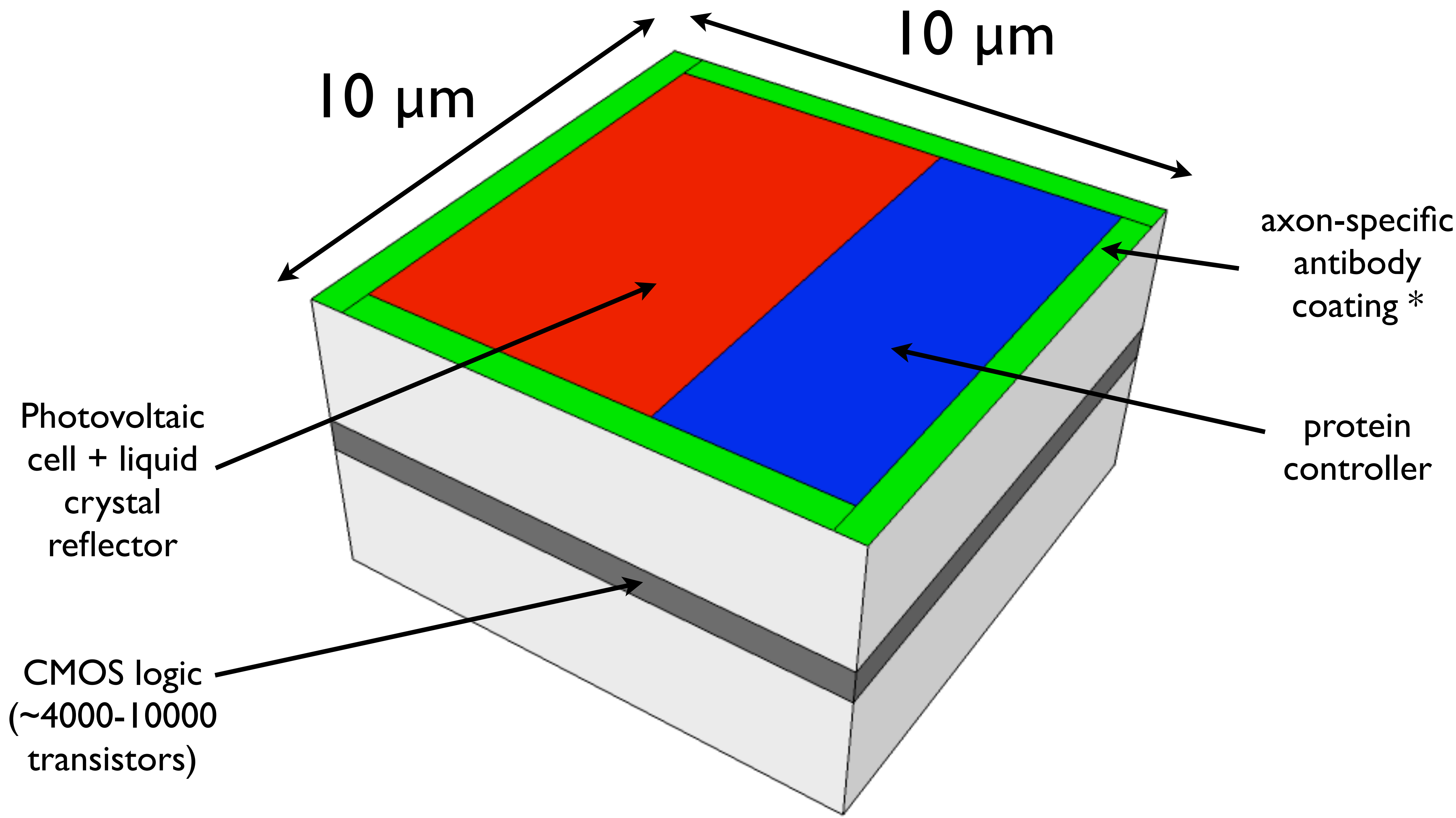

* other 4 sides may be active with antibody or other active function

Antibody-Antigen Binding

- coat with axon-specific antibodies
  - e.g. CD90 http://en.wikipedia.org/wiki/CD90; http://www.epitomics.com/products/product_info/1406/CD90-antibody-2695-1. html

Preliminary Work to use Mesh-based Monte Carlo Simulator with Tissue Experiments

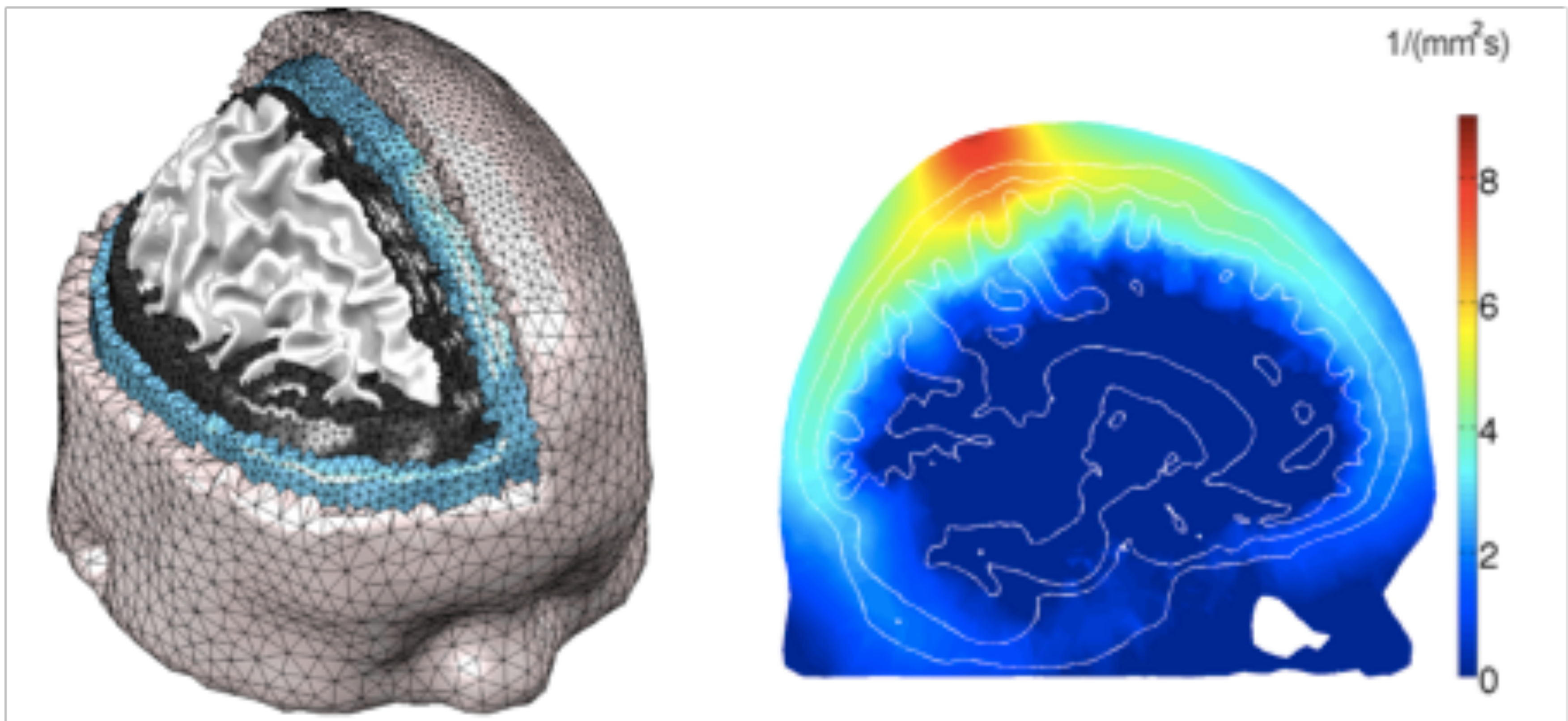

(a) (b)

(Martinos)

350 nW

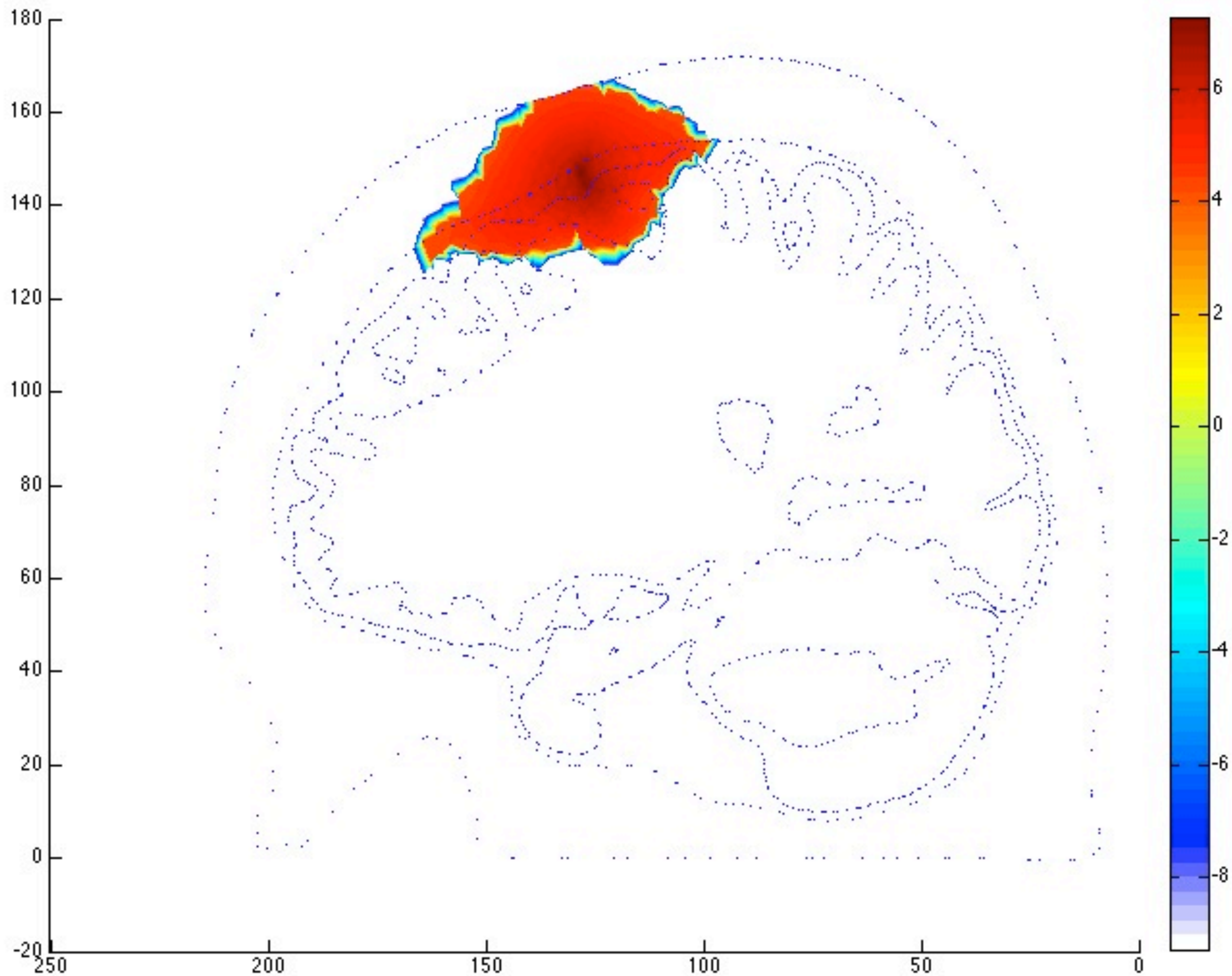

35 nW

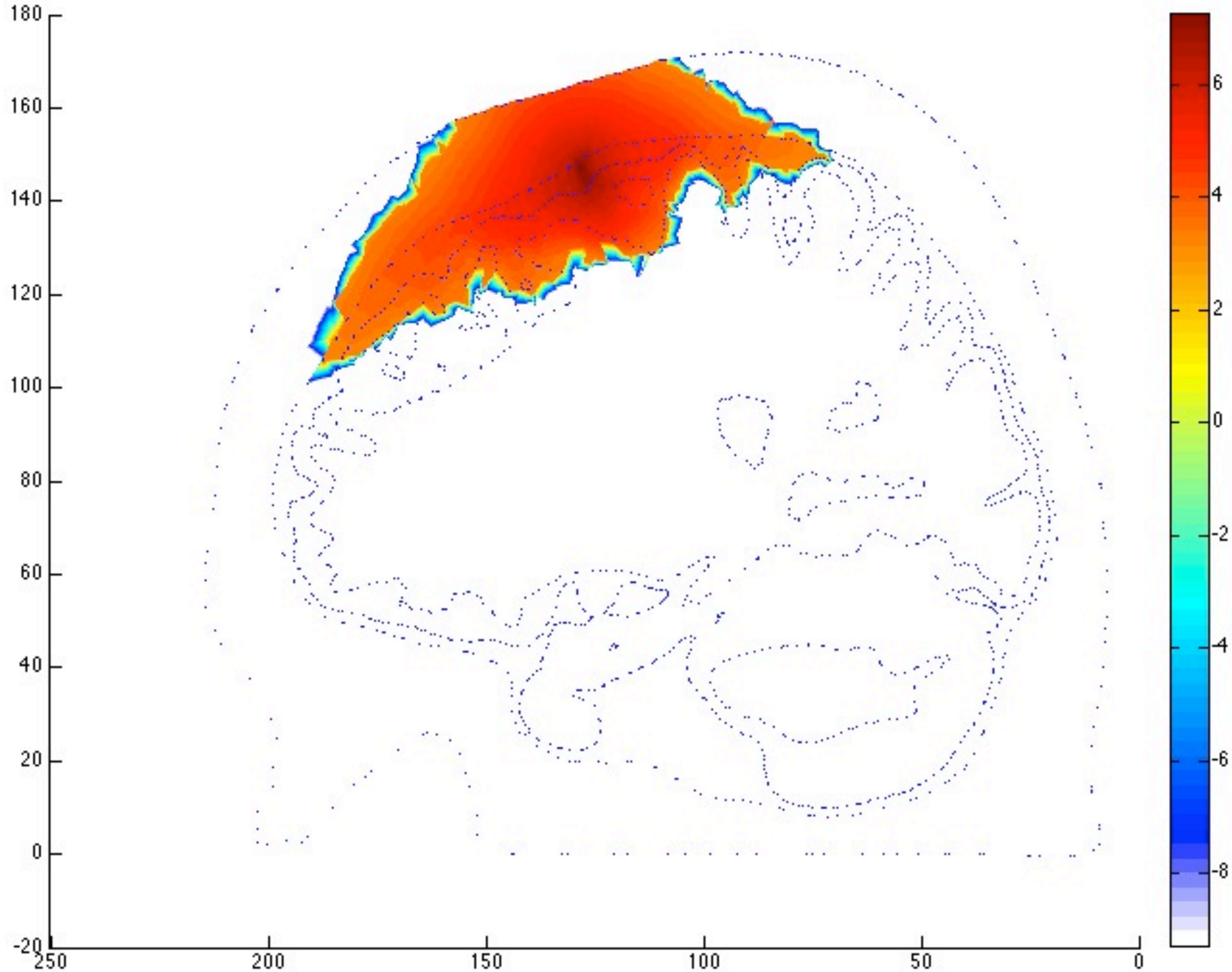

3.5 nW

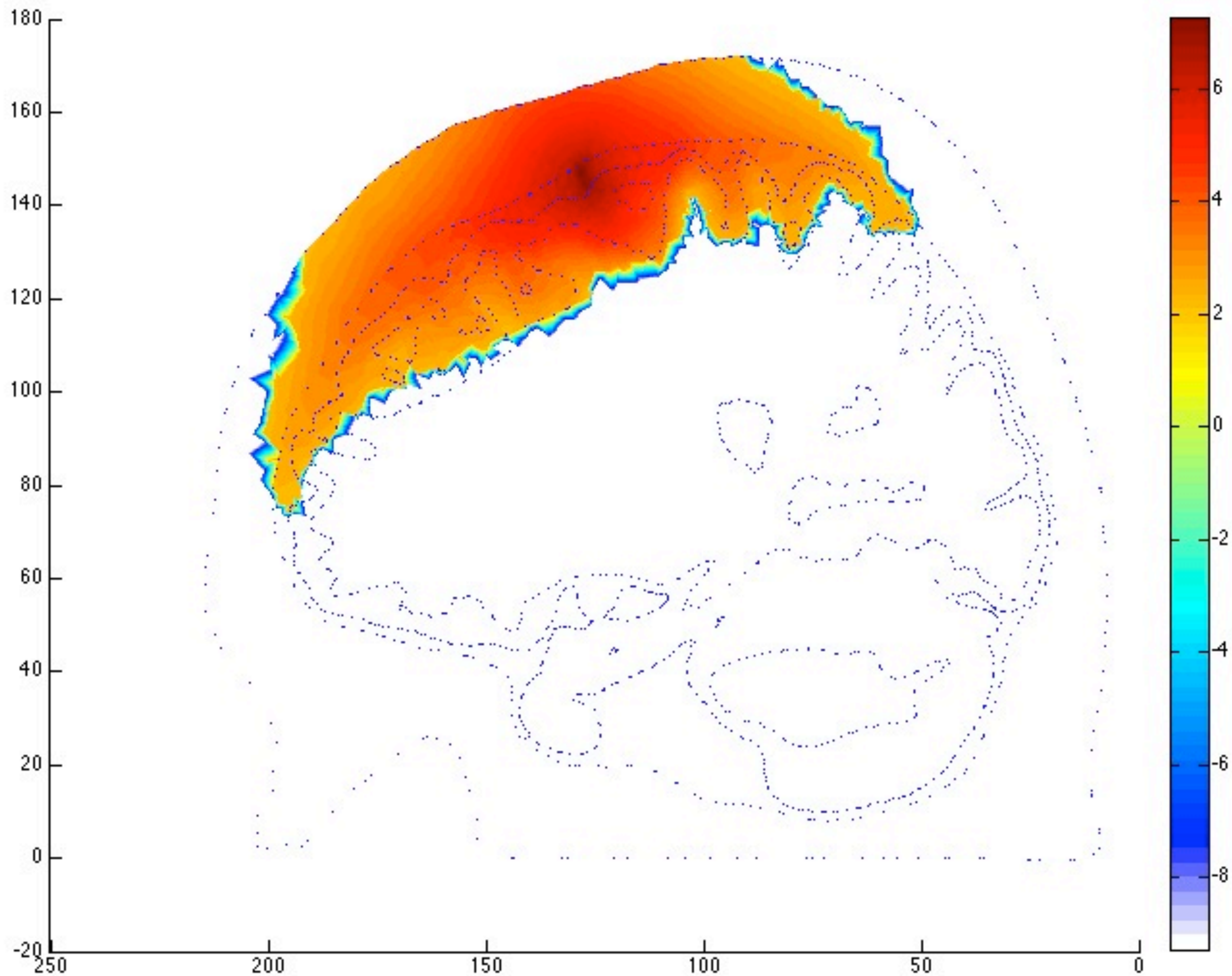

Low-power interaction

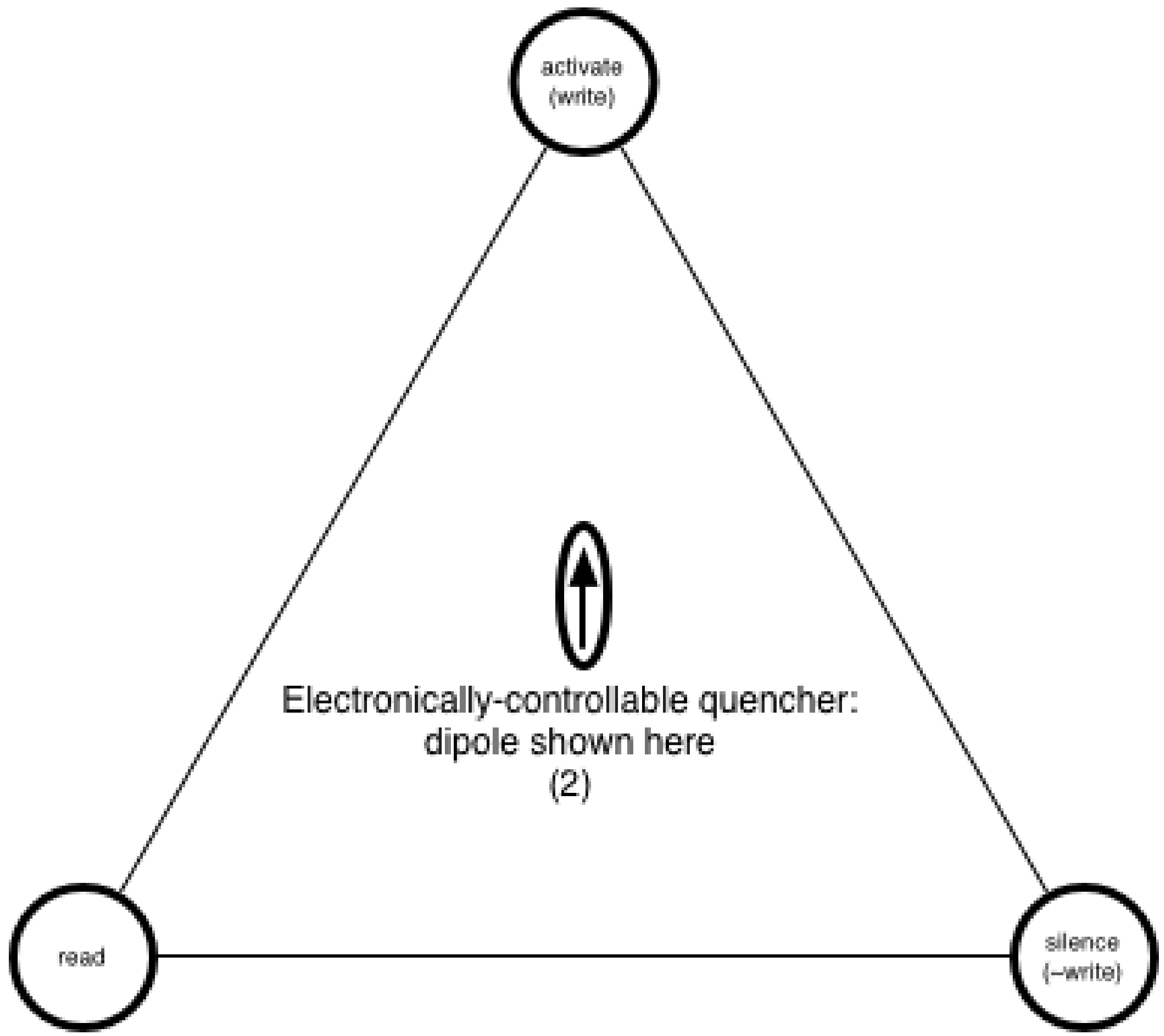

(1) each unit is a protein complex to be shown in more detail
(2) each unit is linked by a peptide/protein complex to obtain a precise spatial relationship amo
units in the membrane and the control dipole.

Quench Controller

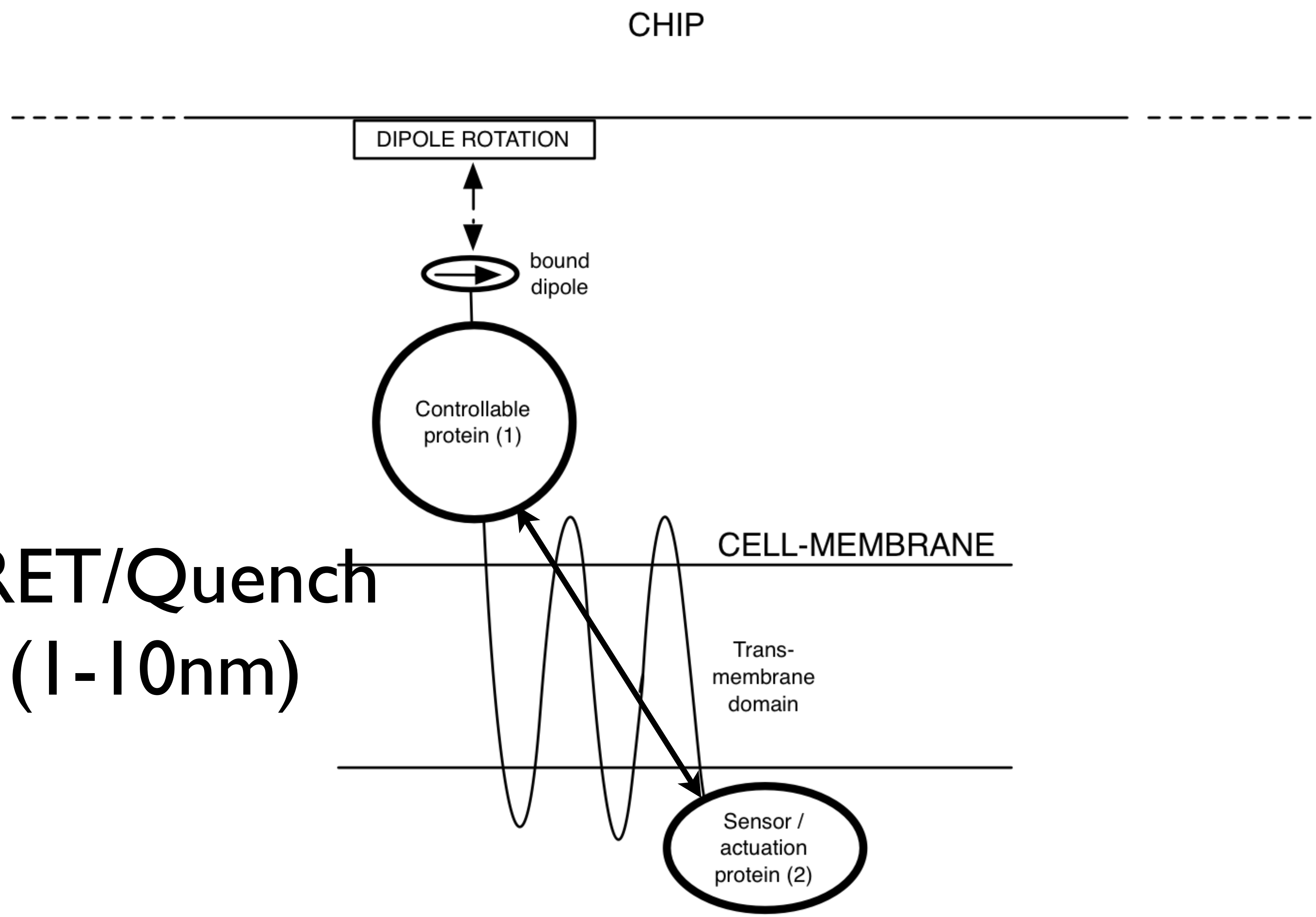

FRET/Quench
(1-10nm)

Nakabayashi et al, Chem Phys Lett 457 (2008) doi: 10.1016/j.cplett.2008.04.018

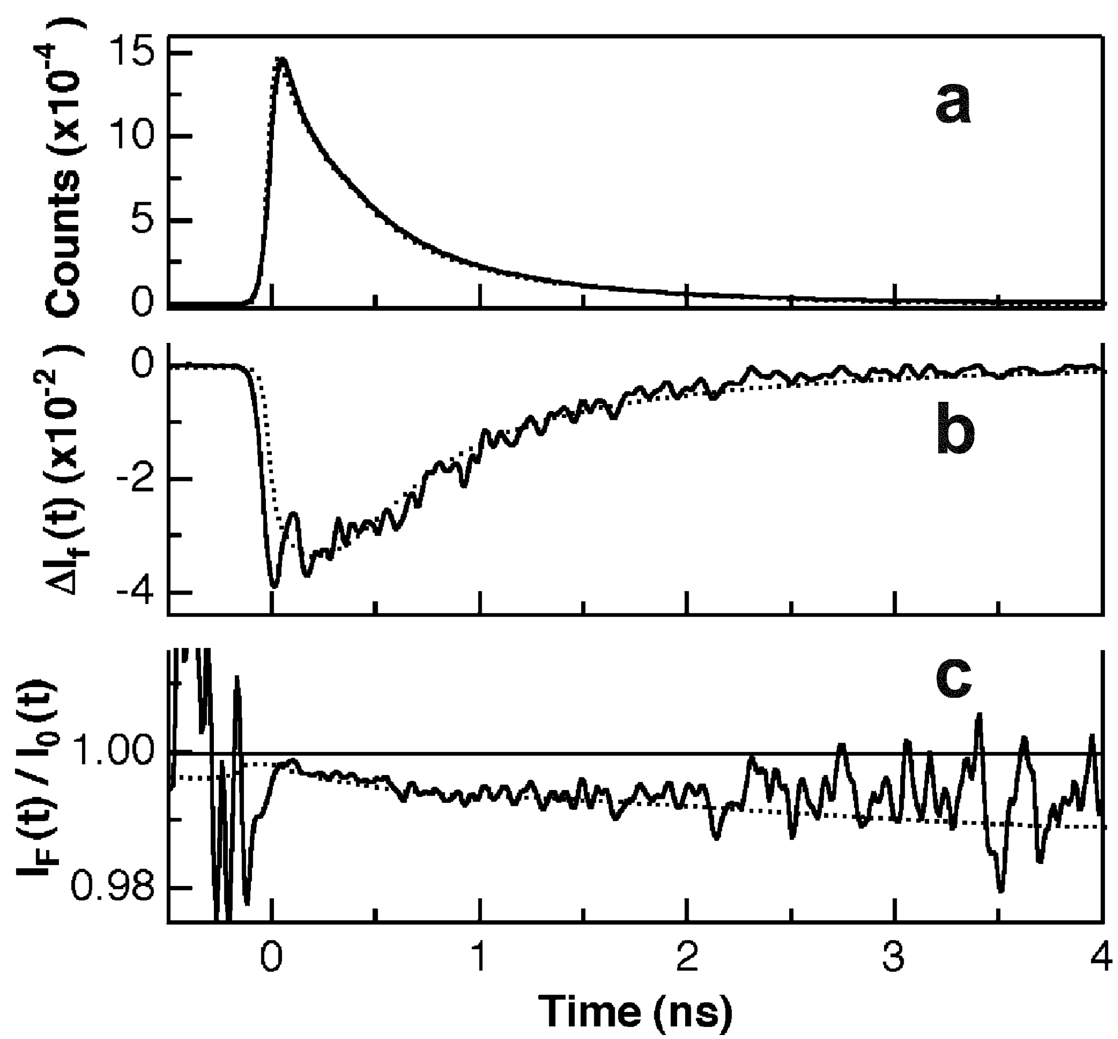

Fig. 4. (a) Fluorescence decay (solid line) of GFPuv5 in a PVA film at zero field. (b) The difference between the decays at 0.7 MV cm^{-1} and at zero field (solid line). (c) The ratio of the decay at 0.7 MV cm^{-1} relative to that at zero field (solid line). The simulated curve is shown in each panel by a dotted line. Excitation and monitoring wavelengths were 440 and 515 nm, respectively.

Becker et al, Nature Materials, v 5 (2006) doi:10.1038/nmat1738

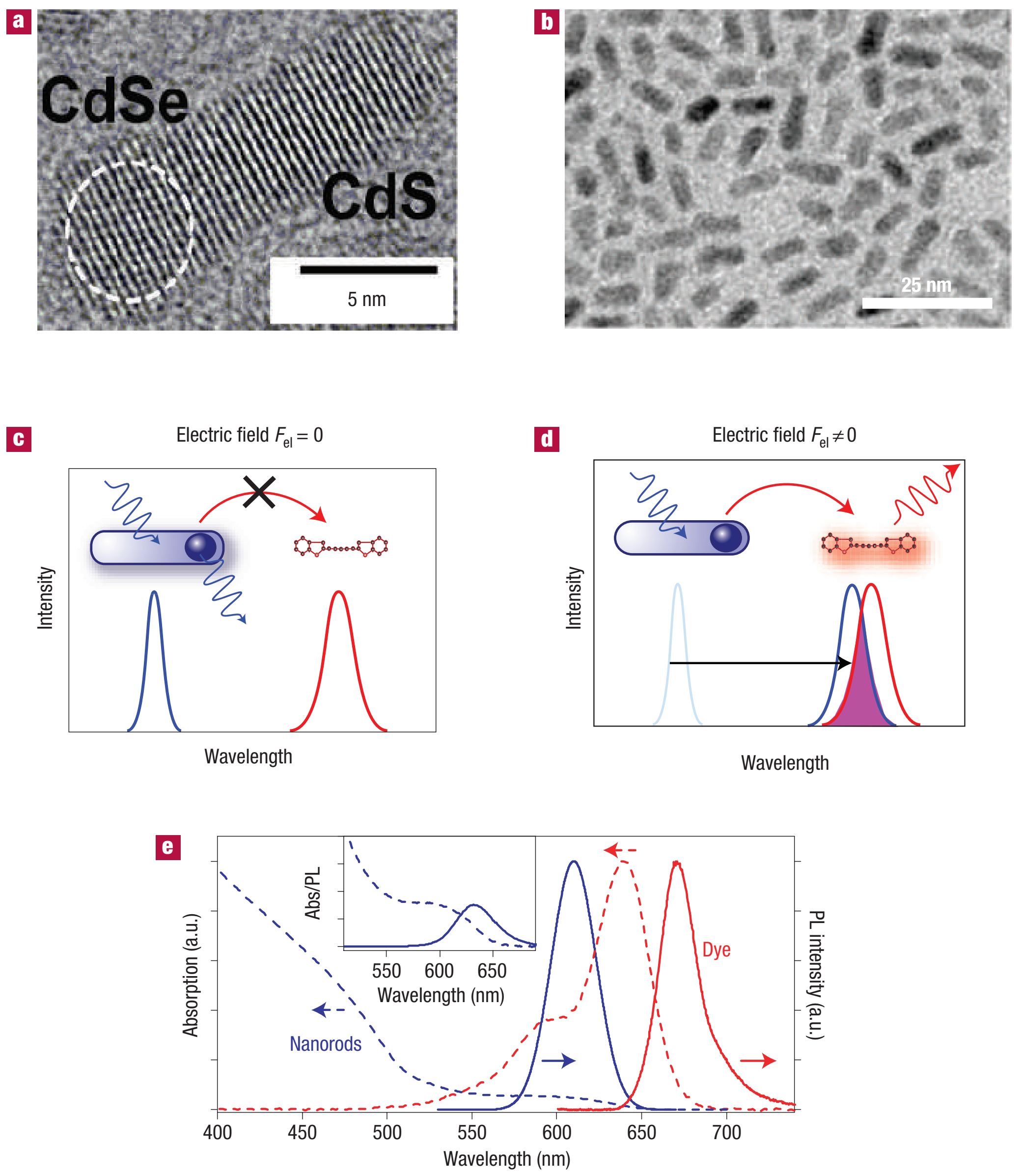

Figure 1 Electrically tunable energy transfer from a single semiconductor nanorod to a dye molecule. **a**,**b**, High-resolution (**a**) and overview (**b**) transmission electron micrographs showing the structure of the CdSe/CdS nanocrystals used. **c**, For a specific set of a single nanocrystal and a single dye molecule no energy transfer occurs because of the lack of spectral overlap between nanocrystal emission and dye absorption. **d**, After application of an electric field, the nanocrystal's PL is red-shifted, resulting in resonance of the nanocrystal and dye transitions. This leads to energy transfer to the dye and subsequent emission. **e**, Absorption (dashed lines) and PL (solid lines) spectra of nanocrystals (blue lines) and dye (red lines). Absorption spectra were taken from chloroform solution at room temperature, whereas emission spectra were taken from polystyrene/dye blends at 50 K. Note the considerable spectral overlap of nanocrystal emission with dye absorption. The inset shows the solution absorption and PL of the nanocrystal excitonic feature.

Dipole Strength Graph

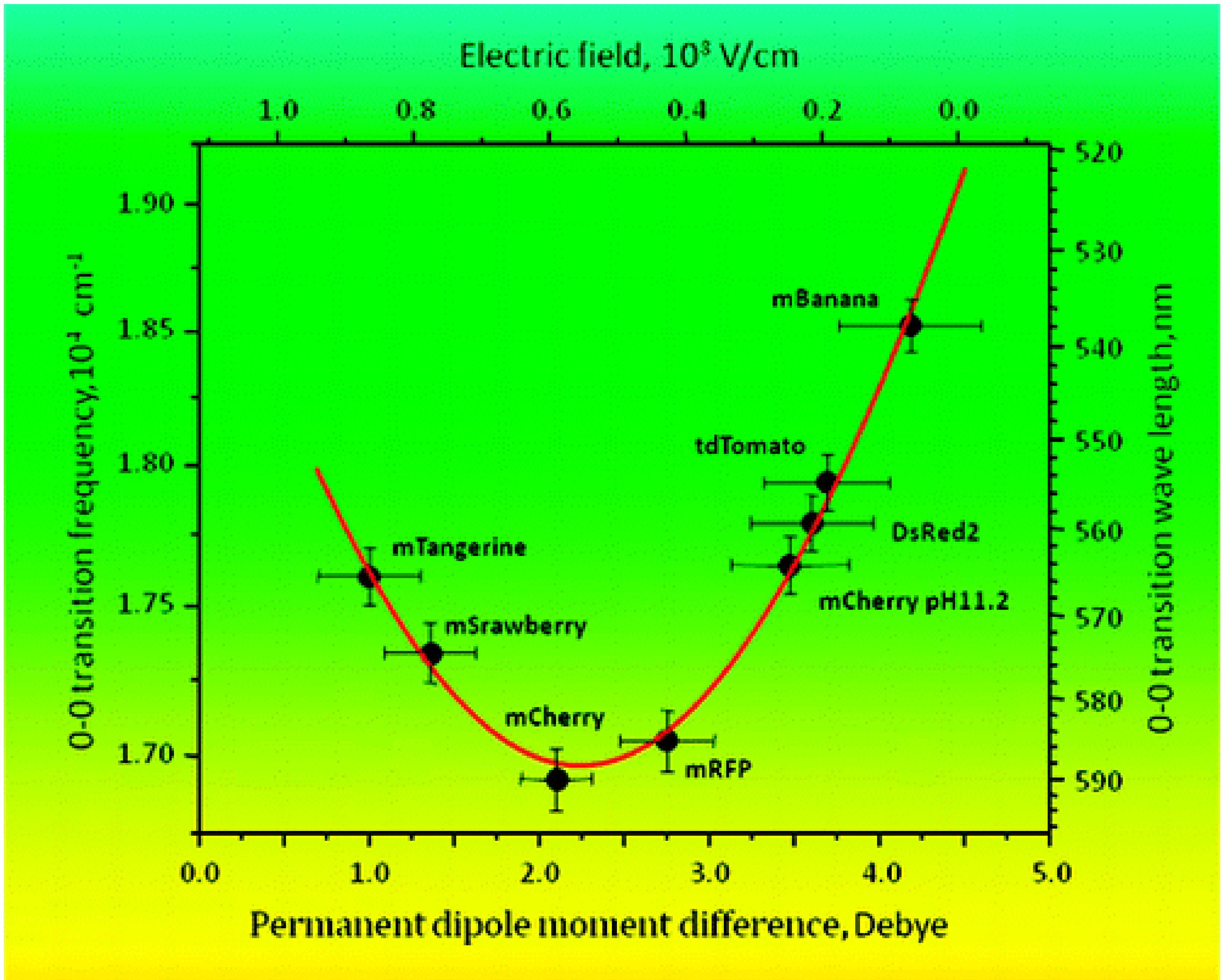

Problems

- Will the mesoscopic scatterer hypothesis apply to the brain?
  - How much can the signal be improved by modulating above 100 kHz?
  - How can one modulate above 100 kHz
- How can a semiconductor chip interact with an light-sensitive protein and power-efficiently digitize a readout protein?
- Can a semiconductor chip be replaced with a biological component or can the power efficiency of a semiconductor chip approach the limits of biology?

Appendix

Glucose

- glucose concentration is 3.6 mM in extracellular fluid
- fat free adipose tissue is 18.8 kJ/kg/day or 110 mW/kg
- high metabolic rate tissue is 226 kJkg/day or 2600 mW/kg
- 100% efficient conversion (2880 kJ/mol) over 10x10 microns, 3.5 microWatt chip would require 1.7 mm/s flux
- range of blood flow is 0.14-0.93 mm/s (impossible)
- state-of-the-art: glucose to gluconolactone or gluconic acid has achieved 1.0-3.3* microWatts/cm2

*B Hansen, Y Liu, and R Yang. Hybrid Nanogenerator for Concurrently Harvesting Biomechanical and Biochemical Energy. *ACS nano*, Jan 2010

S Kerzenmacher, J Ducrée, R Zengerle,
and F von Stetten. An abiotically catalyzed glucose fuel cell for powering medical implants: Reconstructed manufacturing protocol and analysis of performance. *Journal of Power Sources*, 182(1):66–75, 2008